



HAL
open science

Discrete rearranging disordered patterns, part I: Robust statistical tools in two or three dimensions

François Graner, Benjamin Dollet, Christophe Raufaste, Philippe Marmottant

► To cite this version:

François Graner, Benjamin Dollet, Christophe Raufaste, Philippe Marmottant. Discrete rearranging disordered patterns, part I: Robust statistical tools in two or three dimensions. 2007. hal-00160733v2

HAL Id: hal-00160733

<https://hal.science/hal-00160733v2>

Preprint submitted on 21 Dec 2007 (v2), last revised 23 Jan 2008 (v4)

HAL is a multi-disciplinary open access archive for the deposit and dissemination of scientific research documents, whether they are published or not. The documents may come from teaching and research institutions in France or abroad, or from public or private research centers.

L'archive ouverte pluridisciplinaire **HAL**, est destinée au dépôt et à la diffusion de documents scientifiques de niveau recherche, publiés ou non, émanant des établissements d'enseignement et de recherche français ou étrangers, des laboratoires publics ou privés.

Statistical tools to characterize discrete rearranging patterns, in two or three dimensions: cellular materials, assemblies of particles

F. Graner ^a, B. Dollet ^b, C. Raufaste, and P. Marmottant

Laboratoire de Spectrométrie Physique, UMR5588, CNRS-Université Grenoble I, B.P. 87, F-38402 St Martin d'Hères Cedex, France

December 21, 2007

Abstract. Discrete rearranging patterns include cellular patterns, for instance liquid foams, biological tissues, grains in polycrystals; and assemblies of particles such as beads, granular materials, colloids, molecules, atoms. We describe such a pattern as a list of sites, some of which are neighbours. Performing statistics on the links between neighbouring sites, we obtain average quantities (hereafter “tools”) as the result of direct measurements on images. These descriptive tools are flexible and suitable for various problems where quantitative measurements are required, whether in two or in three dimensions. At small scale, they quantify the pattern’s local distortion and rearrangements. At large scale, they help describe a material as a continuous medium. They also provide a direct correspondence between both scales. They thus help formulate elastic, plastic, fluid behaviours in a common, self-consistent language. This facilitates the modelling using continuous mechanics. Since experiments, simulations and models can be expressed in the same language, a direct comparison is easy. As an example, a companion paper (Marmottant, Raufaste and Graner, joint paper) provides an application to foam plasticity.

PACS. 62.20.Fe Deformation and plasticity – 83.10.Bb Kinematics of deformation and flow – 83.80.Iz Emulsions and foams

1 Introduction

1.1 Motivations

Cellular patterns include liquid foams or emulsions (Fig. 1), crystalline grains in polycrystals or biological tissues (Fig. 2). Assemblies of particles (Fig. 3) include collections of beads, molecules, or atoms; granular or colloidal materials; sets of tracers dispersed in a material, such as fluorescent probes or passively carried particles. Despite their tremendous diversity of sizes and physical properties, all these patterns have a common point: they are made of a large number of well-identified individual objects. We call them *discrete patterns*, where the word “discrete” here means the opposite of “continuous”. Other discrete patterns include interconnected networks, of *e.g.* springs, polymers, biological macromolecules, or telecommunication lines.

We define the pattern as *rearranging* if the mutual arrangement of the individual objects can change. This is the case if they can move past each other, for instance

due to mechanical deformation (Figs. 1 or 2a), spontaneous motility (Fig. 2b), or thermal fluctuations (Fig. 3). This is also the case if the number of individual objects can change, for instance due to coalescence or nucleation of bubbles, shrinkage during coarsening of polycrystals or foams, cell division or death (Fig. 2b).

Many tools are available to describe and quantitatively characterise patterns [8]. Here, we introduce tools (listed in Table 1) aimed at describing statistically how the individual objects are arranged with respect to each other. With a few simple measurements performed directly from an image, we extract quantitative information relevant to the size and anisotropy of the pattern. From two successive images in a movie, we extract information regarding the magnitude and direction of deformation rate and rearrangements. All tools here are either static or kinematic, and rely on the image only; that is, they are independent of dynamics (stresses, masses and forces).

Our tools apply to discrete patterns regardless of the size of their individual objects, which can range from nanometer to meters or more. They regard simulations as well as experiments, and should enable quantitative comparison between them. They apply in both 2 or 3 dimensions, and whatever the pattern’s disorder is. The only requirement is that the image should be of sufficient quality to extract

^a Author for correspondence at graner@ujf-grenoble.fr

^b Present address: Department of Science and Technology, University of Twente, P.O. Box 217, 7500 AE Enschede, The Netherlands.

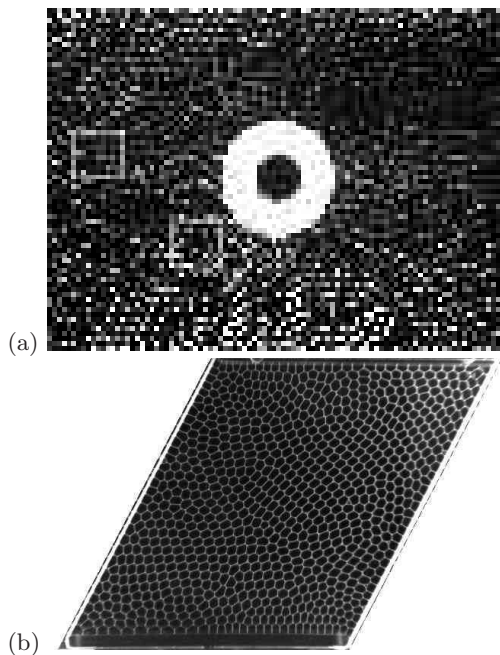


Fig. 1. Liquid foams. (a) Heterogeneous flow: from left to right, around an obstacle [1]; liquid fraction $\sim 10^{-4}$, image width: 15 cm. (b) Homogeneous shear: in a rectangular box, deformed at constant area [2]; liquid fraction $\sim 5 \cdot 10^{-2}$, image width: 18 cm, courtesy C. Quilliet (Univ. Grenoble).

the positions of the centers of each individual object (cell or particle); as well as the list of neighbour pairs (which objects are neighbours).

1.2 Outline of this paper

The main goal of this paper is to present a coherent set of tools, some of which have been already defined and measured in recent separated papers [9, 10, 11, 3, 12, 13, 14, 4]. We try to make it complete and readable; many practical, technical or theoretical details are thus rejected in Appendices. We hope that this presentation is pedagogical enough that the reader can directly use it: if this goal is not reached, we welcome any feedback.

This paper can be read at different levels of increasing difficulty. Most readers will need only the core of the paper, that is, the static description (sections 2.1 and 2.2.1). The description of the pattern evolution requires to read the remaining of section 2. Comparison between different patterns (for instance, experiments and simulations; or various experiments) requires to read section 3. Section 4 is more theoretical: it addresses specific applications of our statistical tools. More precisely, the outline of this paper is as follows.

Sections 2.1 and 2.2.1, valid for all discrete rearranging patterns, introduce our method. The current pattern (that is, a single image) is characterised by its texture \overline{M} (eq. 3). It has been suggested as a tool to describe mechanical deformations by Aubouy *et al.*, but it was already appearing in various contexts, including the order parameters of

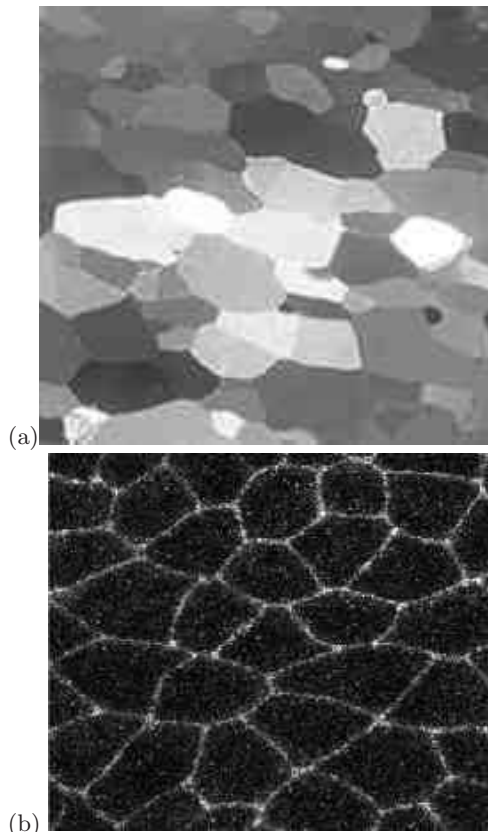


Fig. 2. Other cellular patterns. (a) Grains in a polycrystal of ice which rearranged during ice accumulation [3], image width: 10 cm, courtesy J. Weiss (Univ. Grenoble). (b) Tissue of cells rearranging during the formation of a fruit fly (*Drosophila*) embryo: this thorax epithelium is labeled by the expression of the cell-cell adhesion molecule E-Cadherin-GFP; image width: 160 μm , courtesy Y. Bellaïche (Inst. Curie) [4].

nematics, the microstructure of polymers, or the fabric of grains (see [9] and references therein). Here we refine and hopefully clarify its definition, presenting it step by step, for pedagogical purpose.

The remaining of section 2.2 presents more technical details: how to perform averages in practice, how to represent graphically the texture, how to deal with 2D patterns. Mathematical notations yield more abstract equations, easier to manipulate, valid in both 2D and 3D. Most of this part is developed in Appendices. In particular, for completeness, a detailed appendix recalls all definitions and notations of matrices used in this paper, from basic to difficult.

We then use the texture as the basis on which two other tools are constructed. Section 2.3 describes the changes between two successive images. Firstly, \overline{C} (eq. 12), useful for instance for the flow of a granular material, describes shape (geometry) changes due to the movements of objects relative to each other, without rearrangements. Secondly, \overline{T} (eq. 13), useful for instance for biological cell division or death, describes neighbour (topology) changes due to rearrangements.

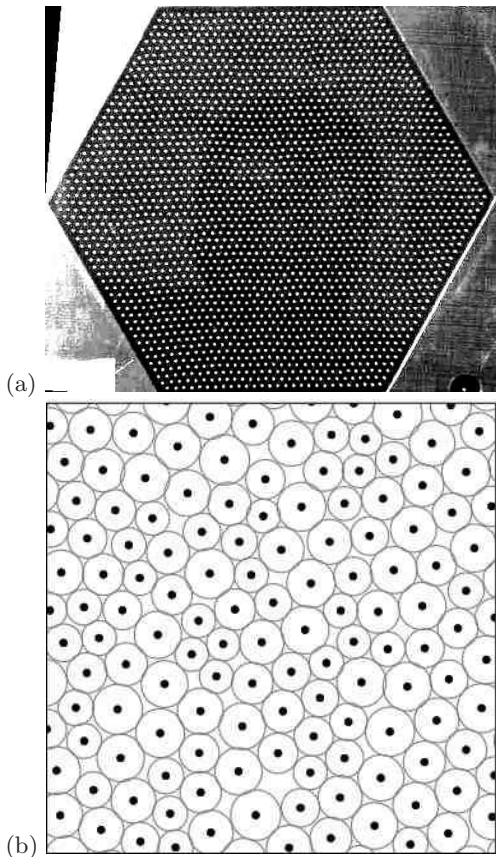


Fig. 3. Assemblies of particles. (a) Beads repelling each other [5]; they are placed on a vibrating loudspeaker, with an effect shown to be equivalent to thermal fluctuations [6]; image size: 11.6 cm, courtesy G. Coupier (Univ. Grenoble). (b) Simulation of amorphous systems of atoms interacting via Lennard-Jones potential [7]: circles indicate each particle's effective radius (here with a 20% dispersity), tangent circles correspond to vanishing interaction force; image size: arbitrary, courtesy A. Tanguy (Univ. Lyon 1).

Section 3 is useful to compare measurements on different patterns; and also for materials which behave as continuous media, that is, where the quantities vary smoothly with space. Each of the three above tools, \overline{M} , \overline{C} and \overline{T} , is rewritten to obtain an equivalent counterpart without any details related with the discrete scale of the pattern. The statistical definition of internal strain \overline{U} (eq. 16), already published [9], is recalled here for completeness. It extends to all types of individual objects displacements, even when these objects are non conserved. In practice, it is measured with a good signal to noise ratio. This is also the case for the statistical velocity gradient \overline{G} (eq. 19), which characterises the variations in space of the velocity, for instance large cell movements during embryo formation. We finally define the statistical topological rearrangement rate \overline{P} (eq. 22).

The second motivation of this paper is to establish a link between discrete description and continuous mechanics. Section 4 discusses when it is possible to identify

Pattern statistics	Texture \overline{M} eqs. (3,9)	Topological changes \overline{T} eq. (13)	Geometrical changes $(\overline{C} + \overline{C}^t)/2$ eq. (12)
Statistical relative deformations	Statistical internal strain \overline{U} eq. (16)	Statistical topological rearrangement rate \overline{P} eq. (22)	Statistical symmetrised velocity gradient \overline{V} eqs. (19,20)
Continuous medium deformations	Current elastic strain $\overline{\varepsilon}_{el}$	Plastic deformation rate $\dot{\overline{\varepsilon}}_{pl}$	Total deformation rate $\dot{\overline{\varepsilon}}_{tot}$

Table 1. Symmetric matrices defined in the text, and numbers of the corresponding equations. For comparison, the last row indicates the deformations defined in continuous mechanics for elastic, plastic and fluid behaviours.

our statistical tools with the usual quantities of continuous mechanics. This suggests a possible way to establish a formulation of continuous mechanics from discrete objects, which is one of our main motivations. Our tools can constitute a coherent language to unify the description of materials which display elastic, plastic and fluid behaviours.

1.3 The example of foams

Our equations are valid in any dimensions. For clarity, we write them in 3D, and show that it is straightforward to rewrite them in 2D, see section 2.2.3. We then use a compact, general expression, see section 2.2.4. We specifically choose to illustrate this paper with 2D images (Figs. 1-3), which are simpler and more common than 3D data.

More precisely, we illustrate each definition on the example of a foam flow (Fig. 1a) [1], which is both our original motivation and the most suitable example. Nitrogen is blown into water with commercial dishwashing liquid. Bubbles enter a channel, of length 1 m (only partly visible on the picture), width 10 cm, and thickness 3.5 mm: a monolayer of bubbles forms (area $A_{bubble} = 16.0 \text{ mm}^2$), sandwiched between two glass plates (quasi-2D foam, liquid fraction less than a percent). It steadily flows from left to right without vertical component (true 2D flow) until it reaches the free end of the channel. Coalescence and ageing are below detection level.

A 3 cm diameter obstacle is inserted into the foam channel. The foam is forced to flow around it, resulting in a spatially heterogeneous velocity field. Different regions simultaneously display different velocity gradients, internal strains, and rearrangement rates, and allow to sample

simultaneously many different conditions. Bubbles naturally act as tracers of all relevant quantities; and on the other hand the foam’s overall behaviour appears continuous. The total deformation rate is partly used to deform bubbles and partly to make them move past each other; the companion paper [15] studies how it is shared between both contributions.

2 Texture and time evolution of links in the discrete pattern

2.1 Ingredients

The pattern is a collection of individual objects. Here we are interested in the relative positions of these objects, not in each object’s shape (although this is related in some cases such as cellular patterns, see Appendix A.3). We thus replace each object by a point called “site”, and reduce the pattern to a network of connected “sites”.

The texture, as all other measurement tools we introduce here, is not rigidly defined. The user should adapt it to the pattern under consideration, and the scientific questions to be answered. For that purpose, the user should begin by deciding what are the relevant links (that is, sites and their connexions), and averaging procedure. This choice is a convention, and thus rather free; once it is chosen, however, it is important to use consistently the same definition to measure the different tools (Appendix A.1). The usual (scalar) measurements, such as the number of neighbours or the number of T1s, depends on the definition. Our statistical tools also depend on the definition, but they are much more robust than scalar measurements (see section 2.3.3). Moreover, their relations (such as eq. 10) are robust, as long as the same definition is used for all measurements.

2.1.1 Links between neighbouring sites

We reduce the pattern to a set of links. Each link’s length and orientation is described by the vector $\ell = (X, Y, Z)$. We set aside the detailed information regarding the actual positions.

However, as an intermediate step, it is usually necessary to measure the position \mathbf{r} of each site, which has three coordinates (x, y, z) . We then need the list of neighbours, that is, pairs of sites which are connected. A pair of neighbour sites of coordinates $\mathbf{r}_1 = (x_1, y_1, z_1)$ and $\mathbf{r}_2 = (x_2, y_2, z_2)$ constitutes a link. The vector:

$$\ell = \mathbf{r}_2 - \mathbf{r}_1, \quad (1)$$

has coordinates $(X, Y, Z) = (x_2 - x_1, y_2 - y_1, z_2 - z_1)$.

In a cellular pattern (Figs. 1,2), it is often advisable to choose as sites each cell’s geometrical center (see Fig. 4a). However, alternative choices exist. For instance, a user interested in studies of dynamics might prefer the center of mass, if different from the geometrical center. Similarly,

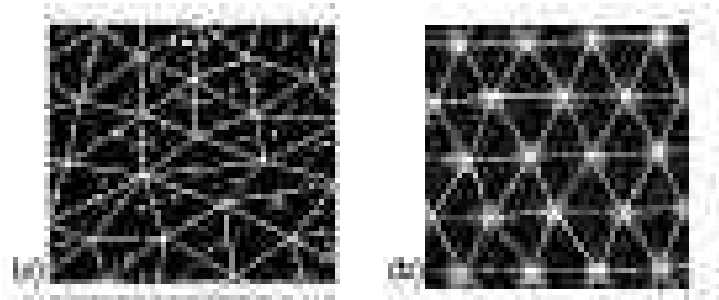


Fig. 4. Definition of sites and links. (a) Cellular pattern. Background: detail from Fig. (2b). Foreground: a site is a cell’s geometrical center; there is a link between two centers if their cells touch. (b) Particle assembly. Background: detail from Fig. (3a). Foreground: a site is a particle’s position; the links are defined as discussed in the text (here a Delaunay triangulation).

a biologist might be more interested in the cell’s centrosome or nucleus. Note that we do not advise to use a definition based on vertices (see Appendix A.3). When two cells touch each other it defines that their sites are connected. This is unambiguous if cells walls are thin. This is the case for grains in polycrystals, cells in an epithelium, or in a foam with low amount of water (Figs. 1a,2). If cells walls are thick, as is the case in a foam with a higher amount of water (Fig. 1b), different definitions of neighbours are possible. For instance, two cells are defined as neighbours if their distance is smaller than a given cut-off. Or, if they are neighbours on a skeletonized image; that is, after an image analysis software has reduced cell walls to one pixel thick black lines on a white background. If cell walls are too thick, cells are really separated (as in a bubbly liquid, where bubbles are round and far from each other) and can be treated like the particles, which we now discuss.

If each object is a particle (as in Fig. 3) it is natural to choose its center as site (see Fig. 4b). There are various possible choices for the links. Whatever the chosen definition, it is important that each particle has only a finite number of neighbours. In a first case (Fig. 3b), the average distance between particles is comparable to their average radius; for instance, for a dense (also called compact or jammed) colloid or granular material. We then recommend to define that two particles are linked if their distance is less than a chosen cut-off. For hard spheres, this cut-off should be the sphere’s radius plus a small tolerance. In the opposite case, the average distance between particles is much larger than their average radius (Fig. 3a); for instance, for a decompacted colloid or granular material. We then recommend to recreate a cellular pattern by attributing to each particle its Voronoi domain (the set of points surrounding this particle, closer to it than to any other particle). One then chooses to define that two particles are linked if their Voronoi domains touch; this is called the “Delaunay triangulation” of the particles.

If the pattern is a network, it is natural to choose the nodes as sites. The connexions are physically materialised, and thus unambiguously defined.

2.1.2 Averaging

The present tools aim at describing the collective properties of links. In what follows, $\langle \cdot \rangle$ denotes the average over a set of links relevant to the user: $\langle \cdot \rangle = N_{tot}^{-1} \Sigma(\cdot)$ where the sum is taken over the number N_{tot} of such links.

Choosing to average over a small number N_{tot} of links yields access to detailed local information. For instance, the local heterogeneity of a sample of ice (Fig. 2a) can be measured by including the links around one single grain, then performing a comparison between different grains [3]. Similarly, to study the anisotropy of a cell which divides, one can include only the links starting at this cell's center (Fig. 2b).

On the other hand, choosing a large number N_{tot} of links yields better statistics. To detect the overall anisotropy of an ice sample (Fig. 2a) or an epithelium (Fig. 2b) requires averaging over all links contained in the whole image. This enables a comparison with other samples [3].

If the system is homogenous in space, an average improves the statistics. For instance, in a homogenous sheared foam, it makes sense to consider that all bubbles play a similar role, and average over the whole foam (Fig. 1b). Even if the system is invariant over only one direction of space, one can average over this direction. Similarly, in a flow which is invariant in time, one can average over time (Fig. 1a). For instance, here, figures are prepared with $A_{box} = 37 \text{ mm}^2$ and $\tau = 750$ successive video images (we checked that these choices do not affect the equations presented below); thus millions of bubbles can be available: a time average yields good statistics even if only a small part (*i.e.* few links) of each image is included (Fig. 6).

The scale of study determines the number of links included. Performing the same analysis at different scales enables to obtain multi-scale results [12,3,14]. For instance, we can measure the dependence of pattern fluctuations with scale for particle assemblies (Fig. 3).

Appendix A.1 presents some technical details, especially regarding the boundaries of the averaging region, which can be treated as sharp or smooth.

2.2 Texture \bar{M} : current state of the pattern.

2.2.1 Definition and measurement

For a given link, the vector $\ell = (X, Y, Z)$ indicates its length and direction. These are the informations we want to average. However, ℓ has a sign, *i.e.* an orientation. It is not only irrelevant, since ℓ and $-\ell$ play the same physical role; but also problematic: an average over several ℓ s will yield a result which depends on this arbitrary choice of signs (and, in practice, if there are enough links, the average $\langle \ell \rangle$ turns out to be close to zero).



Fig. 5. Measurement of texture. Snapshots of two regions selected in Fig. (1a): the foam is nearly isotropic in A, not in B. From the statistical analysis of links (lines), and time average over several images, we compute the corresponding \bar{M} . We represent it by an ellipse with axes proportional to the eigenvalues: in A it is nearly circular. Thin lines indicate the axes with positive eigenvalues (*i.e.* here all axes).

The number $\ell^2 = X^2 + Y^2 + Z^2$ does not depend on any arbitrary sign and thus has a physically relevant average, $\langle \ell^2 \rangle = \langle X^2 + Y^2 + Z^2 \rangle$. It reflects the average square link length, but loses the information of direction.

To combine the advantages of both, one can simply store the same information in an array independent of the link sign, as follows:

$$\begin{pmatrix} X^2 & XY & XZ \\ YX & Y^2 & YZ \\ ZX & ZY & Z^2 \end{pmatrix}. \quad (2)$$

Averaging it, we easily construct the following array, called *texture* [9]:

$$\bar{M} = \begin{pmatrix} \langle X^2 \rangle & \langle XY \rangle & \langle XZ \rangle \\ \langle YX \rangle & \langle Y^2 \rangle & \langle YZ \rangle \\ \langle ZX \rangle & \langle ZY \rangle & \langle Z^2 \rangle \end{pmatrix}. \quad (3)$$

It is expressed in m^2 . As required, it stores the same information regarding the current pattern [10,11,3,12,14,13]: the square length, readily visible as the sum of diagonal terms; the orientation and magnitude of anisotropy, as we discuss below; but not the sign of links.

2.2.2 Diagonalisation and representation

By construction, \bar{M} is a matrix with symmetric off-diagonal terms ($XY = YX$, etc...). It can thus be diagonalised (see Appendix B.2 for details):

$$\text{diag } \bar{M} = \begin{pmatrix} \lambda_1 & 0 & 0 \\ 0 & \lambda_2 & 0 \\ 0 & 0 & \lambda_3 \end{pmatrix}. \quad (4)$$

Its three eigenvalues λ_i ($i = 1, 2$ or 3) are strictly positive. Their sum, $\text{Tr} \bar{M}$, is exactly $\langle \ell^2 \rangle$. In practice, they usually have the same order of magnitude, $\lambda_i \approx \langle \ell^2 \rangle / 3$.

In a true 3D pattern, \bar{M} has strictly positive eigenvalues (except in unphysical examples). Thus its inverse \bar{M}^{-1} always exists (eq. 49).

$\overline{\overline{M}}$ can be represented as an ellipsoid, which axes directions are that in which $\overline{\overline{M}}$ is diagonal, represented as thin lines on Fig. (5). Each ellipsoid's axes length is proportional to the corresponding λ_i . That is, the direction in which links are longer is represented by the direction of ellipsoid elongation: the greater the pattern's anisotropy, the more elongated the ellipsoid. The square link length $\langle \ell^2 \rangle$ is reflected in the size of the ellipsoid, more precisely as the square root of the sum of the three axes lengths; it is thus *not* proportional to the ellipsoid's volume.

If the texture is measured at several regions of the image, it is represented as several ellipsoids, that is, a map of the texture field $\overline{\overline{M}}(\mathbf{R}, t)$ (Fig. 6). The same analysis can be performed at larger scale to decrease the noise due to fluctuations (Fig. 6a), or at smaller scale to evidence more details of the spatial variations (Fig. 6c). The intermediate scale (Fig. 6b) corresponds to the one chosen as reference throughout this paper.

When the pattern is isotropic, so is its texture. It is thus diagonal in any system of axes, and the three λ_i s are exactly equal, $\lambda_i = \langle \ell^2 \rangle / 3$:

$$\begin{aligned} \overline{\overline{M}}^{\text{isotropic}} &= \begin{pmatrix} \frac{\langle \ell^2 \rangle}{3} & 0 & 0 \\ 0 & \frac{\langle \ell^2 \rangle}{3} & 0 \\ 0 & 0 & \frac{\langle \ell^2 \rangle}{3} \end{pmatrix} \\ &= \frac{\langle \ell^2 \rangle}{3} \begin{pmatrix} 1 & 0 & 0 \\ 0 & 1 & 0 \\ 0 & 0 & 1 \end{pmatrix}. \end{aligned} \quad (5)$$

That is, the texture of an isotropic pattern contains only the information of length: $\overline{\overline{M}} = \langle \ell^2 \rangle \overline{\overline{I}}_3 / 3$, where $\overline{\overline{I}}_3$ is the identity matrix in 3D. It is represented as a sphere. In that case, all axes are equivalent (or “degenerated”), see also section 2.2.3.

2.2.3 Two dimensionnal case

If the pattern under consideration is contained in a plane, as are most experimental images, we turn to a 2D notation. As mentioned, this is straightforward:

$$2D : \quad \overline{\overline{M}} = \begin{pmatrix} \langle X^2 \rangle & \langle XY \rangle \\ \langle YX \rangle & \langle Y^2 \rangle \end{pmatrix}. \quad (6)$$

There exist two orthogonal axes (eigenvectors) in which $\overline{\overline{M}}$ would be diagonal:

$$2D : \quad \text{diag } \overline{\overline{M}} = \begin{pmatrix} \lambda_1 & 0 \\ 0 & \lambda_2 \end{pmatrix}. \quad (7)$$

with strictly positive λ_i , ($i = 1$ or 2). It is represented by an ellipse: this is what we use for the illustrations of this paper (Fig. 5). Its inverse $\overline{\overline{M}}^{-1}$ always exists (eq. 49).

If we call $\langle \ell_+ \rangle$ the r.m.s. length of links in the direction of elongation (say, 1) and $\langle \ell_- \rangle$ the r.m.s. length of links in

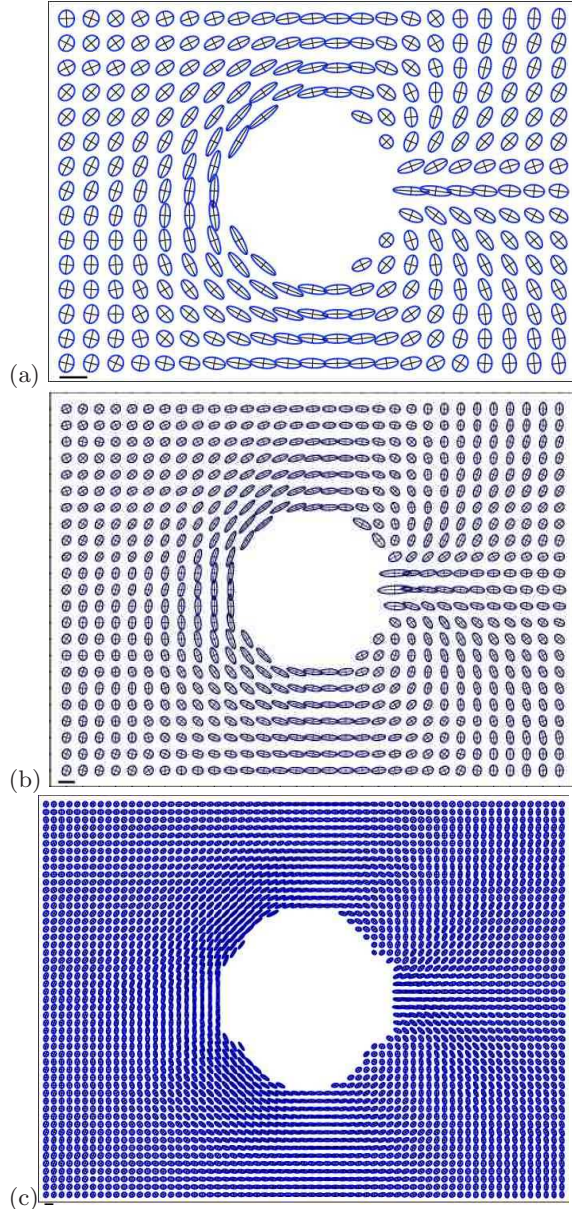


Fig. 6. Map of the texture measured in each region of the foam flow (Fig. 1a). The area V_{box} of each averaging box corresponds to (a) 3, (b) 1 and (c) 0.3 bubbles; since there are 1000 movie images, and 3 times more links than bubbles [16], this corresponds to averages over 10^4 , $3 \cdot 10^3$ and 10^3 links, respectively. Scale: actual image size, 15 cm \times 10 cm; $\overline{\overline{M}}$ (ellipses): bar = 10 mm².

the direction of compression (say, 2), then $\lambda_1 \approx \langle \ell_+^2 \rangle / 2$ and $\lambda_2 \approx \langle \ell_-^2 \rangle / 2$. When the pattern is isotropic, its texture is diagonal with any choice of axes:

$$\begin{aligned} \overline{\overline{M}}^{\text{isotropic}} &= \begin{pmatrix} \frac{\langle \ell^2 \rangle}{2} & 0 \\ 0 & \frac{\langle \ell^2 \rangle}{2} \end{pmatrix} \\ &= \frac{\langle \ell^2 \rangle}{2} \begin{pmatrix} 1 & 0 \\ 0 & 1 \end{pmatrix}, \end{aligned} \quad (8)$$

That is, $\overline{\overline{M}} = \langle \ell^2 \rangle \overline{\overline{I_2}} / 2$, where $\overline{\overline{I_2}}$ is the identity matrix in 2D. It is represented by a circle. Here again, all axes are equivalent (or “degenerated”); see for instance A in Fig. (5) or far left and right of Fig. (6): the ellipses are nearly circular and their thin lines lose their signification.

2.2.4 Compact notation

The array defined in eq. (2) is the matrix one can build using only the vector ℓ . It is sometimes called the “tensor product” (or equivalently “outer product”) of ℓ by itself, and denoted by $\ell \otimes \ell$. For the sake of generality and brevity, from now on we use this compact notation, valid in all dimensions (see Appendix B.3 for more details).

A matrix, like a vector, is a tensor which can be manipulated as a whole, independently of its detailed components. Thus several of its properties are independent from the choice of the axes of coordinates. It can be averaged, so that we rewrite both eqs. (3) and (6) as:

$$\overline{\overline{M}} \equiv \langle \ell \otimes \ell \rangle. \quad (9)$$

A physical origin of this expression is discussed in Appendix B.4.

2.3 Time evolution

The time evolution of $\overline{\overline{M}}$ helps define two other tools, $\overline{\overline{C}}$ and $\overline{\overline{T}}$, which can be measured on a movie.

2.3.1 Changes of texture with time

By differentiating eq. (9) (see details in the Appendix C.1), we can write approximately how $\overline{\overline{M}}$ varies:

$$\frac{\partial \overline{\overline{M}}}{\partial t} = -\nabla \cdot \overline{\overline{J_M}} + \left(\overline{\overline{C}} + \overline{\overline{C}}^t \right) + \overline{\overline{T}}, \quad (10)$$

Physically, these three terms have the following meaning. In the time interval Δt between two successive images, some links enter or exit the region of averaging; some links change their length or direction; some links are created or destroyed. The first term is now discussed briefly. Both other terms play a role in what follows and we discuss them in more details (sections 2.3.2 and 2.3.3).

Here $\overline{\overline{J_M}}$ is the flux of advection, that is, the transport of texture. It counts the rate at which links enter or exit through the sides of the region of averaging. Technically, it is a rank-three tensor (*i.e.* with 3 indices): for more details see ref. [17] and Appendix B.3. In a good approximation, $\overline{\overline{J_M}} \simeq \mathbf{v} \otimes \overline{\overline{M}}$, where \mathbf{v} is the local average velocity. Its divergence $\nabla \cdot \overline{\overline{J_M}}$ counts the net balance between links that enter and exit; it vanishes if $\overline{\overline{M}}$ is spatially homogeneous, or at least is constant along a flux line; it also vanishes if the local average velocity is zero.

2.3.2 Geometrical texture changes: $\overline{\overline{C}}$

$\overline{\overline{C}}$ describes the changes in the pattern’s shape, that is, geometry: rotation or elongation of the pattern. It reflects relative movements: it is insensitive to a global, collective translation. It can thus characterise at which rate, and in which direction, a cell deforms. It is useful in particular for theoretical purposes, or as an intermediate step to introduce $\overline{\overline{G}}$ (section 3.3.1).

$\overline{\overline{C}}$ is based on the links which, on both successive images, exist (*i.e.* do not undergo topological rearrangement) and belong to the region of averaging (*i.e.* are not advected). These links may change in length and direction (Fig. 7). We obtain each link’s contribution directly from eq. (9) and average it:

$$\left\langle \frac{d(\ell \otimes \ell)}{dt} \right\rangle = \left\langle \ell \otimes \frac{d\ell}{dt} + \frac{d\ell}{dt} \otimes \ell \right\rangle. \quad (11)$$

From eq. (11) we define (see details in the Appendix C.1):

$$\begin{aligned} \overline{\overline{C}} &= \left\langle \ell \otimes \frac{d\ell}{dt} \right\rangle \\ &= \left(\begin{array}{ccc} \langle X \frac{dX}{dt} \rangle & \langle Y \frac{dX}{dt} \rangle & \langle Z \frac{dX}{dt} \rangle \\ \langle X \frac{dY}{dt} \rangle & \langle Y \frac{dY}{dt} \rangle & \langle Z \frac{dY}{dt} \rangle \\ \langle X \frac{dZ}{dt} \rangle & \langle Y \frac{dZ}{dt} \rangle & \langle Z \frac{dZ}{dt} \rangle \end{array} \right). \end{aligned} \quad (12)$$

Its units are in m^2s^{-1} . Its transposed is $\overline{\overline{C}}^t = \langle d\ell/dt \otimes \ell \rangle$.

Its symmetric part $\left(\overline{\overline{C}} + \overline{\overline{C}}^t \right) / 2$ has a positive eigenvalue in the direction of extension, and a negative one in the direction of compression. In a region of shear, it can thus be plotted as an ellipse with one thin line drawn on it, similar to a “coffee bean” (Fig. 7). We can plot a map of $\left(\overline{\overline{C}} + \overline{\overline{C}}^t \right) / 2$: it is similar to that of $\overline{\overline{V}}$ (Fig. 10). In case of dilation, for instance for cell growth, all its eigenvalues are positive.

2.3.3 Topological texture changes: $\overline{\overline{T}}$

$\overline{\overline{T}}$ reflects the topological changes, that is, changes in the list of links: creation and destruction, that is, source term of the texture. For details see the Appendix C.1. Briefly, each link ℓ_a which appears between two successive images (separated by a time interval Δt) has a contribution given by eq. (2), noted $\ell_a \otimes \ell_a$; and similarly the contribution of a link which disappears is noted $\ell_d \otimes \ell_d$. Averaging over all links which appear or disappear between successive images defines $\overline{\overline{T}}$ as:

$$\overline{\overline{T}} = \dot{n}_a \langle \ell_a \otimes \ell_a \rangle - \dot{n}_d \langle \ell_d \otimes \ell_d \rangle. \quad (13)$$

Here ℓ_a (resp. ℓ_d) is a link at the time it appears (resp. disappears). The quantity \dot{n}_a (resp. \dot{n}_d), expressed in s^{-1} , is *not* the time derivative of a physical quantity (which we

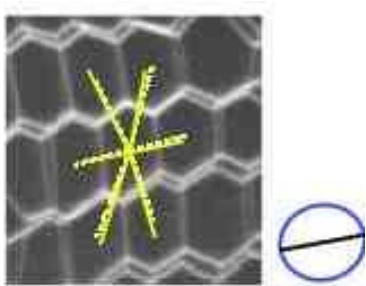


Fig. 7. Changes in the shape of links (geometry). In a first snapshot of a small region of the foam, links are represented by dashed lines. The same bubbles are tracked on a next image, with links represented by solid lines. To evidence how each link changes, we have removed the overall translation (which plays no role here), and superimposed both snapshots. We calculate $(\bar{C} + \bar{C}^t)/2$ and plot it as a coffee bean: an ellipse with a thin line indicating the positive eigenvalue (direction of extension).

would note d/dt). It is the rate of link appearance (resp. disappearance), per unit time and per existing link. If \dot{n}_a and \dot{n}_d are equal, their inverse is the average link's life expectancy.

$\bar{\bar{T}}$ has been introduced in ref. [14]. It is expressed in m^2s^{-1} . It characterises the total effect on the pattern of all topological changes occurred between two images (and can also be averaged over a whole movie). By construction it is symmetric, like \bar{M} : it can thus be diagonalized and represented as an ellipsoid. It includes information of frequency, size, direction and anisotropy for all kinds of topological changes. However, as we now discuss, the user might be interested in studying separately the contributions of the different processes [4].

Neighbour exchanges (Fig. 8a,b), also called “T1” in the case of cellular patterns [18,16], preserve the sites; in 2D, they also preserve the number of links, $\dot{n}_a = \dot{n}_d$. $\bar{\bar{T}}$ usually is mostly deviatoric (Appendix B.1), with both positive and negative eigenvalues, in directions correlated with the appearing and disappearing links. Note that the eigenvectors are exactly orthogonal, while the appearing and disappearing links need not be: thus eigenvectors are not strictly parallel to links, especially when $\bar{\bar{T}}$ is measured as an average over several individual topological processes. We can plot a map of $\bar{\bar{T}}$ for our flowing foam example: it is similar to that of $\bar{\bar{P}}$ (Fig. 11).

The disparition of a site (Fig. 8c) corresponds in foams to a bubble which shrinks, also called “T2” [18,16]; and in epithelia to a cell which dies, or exits the epithelium plane. The reverse process is a site nucleation. Both processes have an approximately isotropic contribution to $\bar{\bar{T}}$.

The coalescence of two sites (Fig. 8d) corresponds in foams to the breakage of a liquid wall between two bubbles, with a net balance of minus one site [19]. The reverse process corresponds in epithelia to a cell division, and results in one more site [20]. When the number of sites decreases (resp. increases), so does the number of links, and

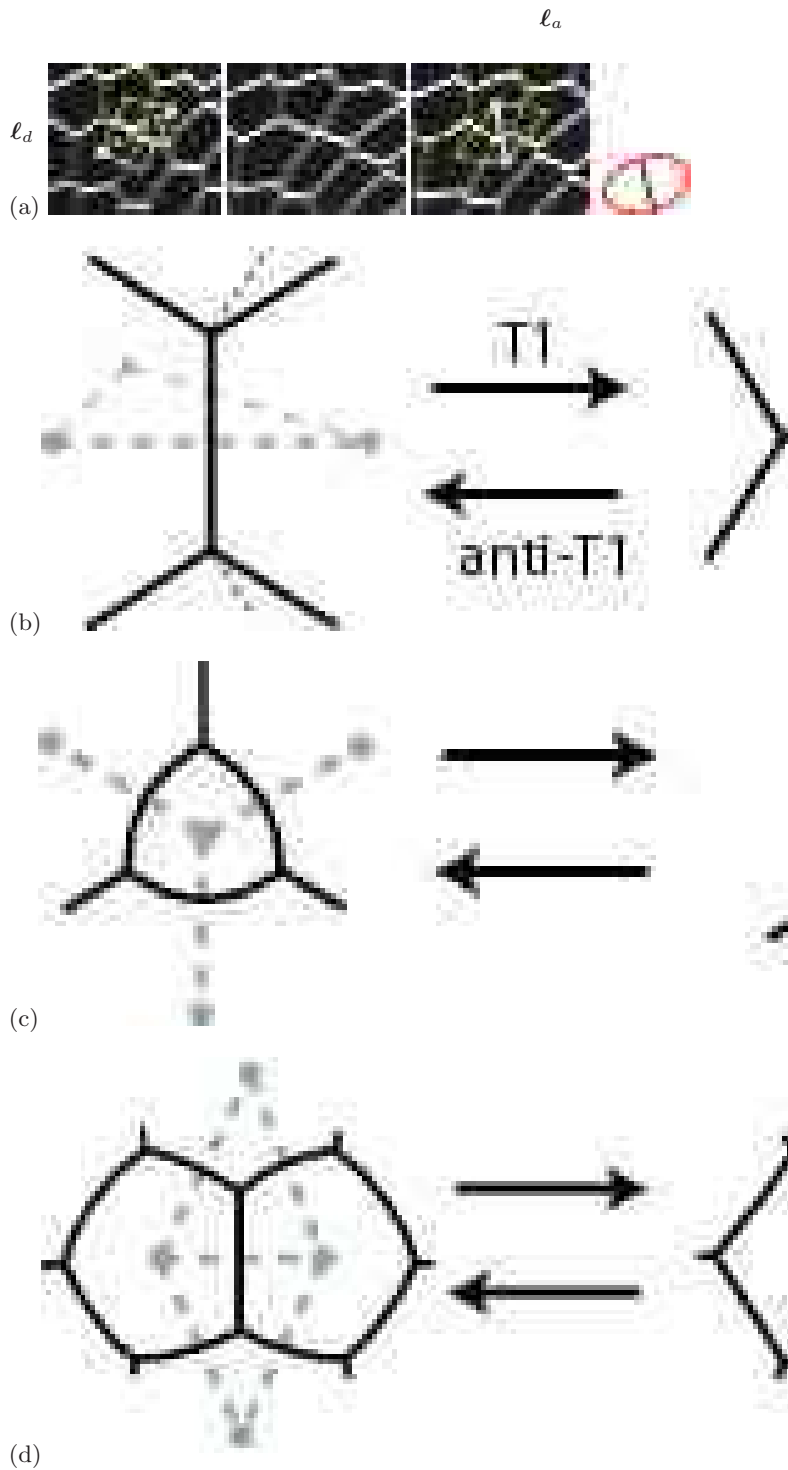


Fig. 8. Changes in the list of links (topology). They are here illustrated by cellular patterns but are much more general. (a) Neighbour exchange in 2D: snapshots extracted from a dry foam [15], one link disappears (dashes) and another appears (thick grey line); and corresponding representation of $\bar{\bar{T}}$ as an ellipse, where a thin line indicates the positive eigenvalue. (b) Same, sketched in 3D: three links (hence 3 faces) disappear and one appears. (c) Site disparition, in 2D or 3D: all its links disappear. (d) Coalescence of two sites, in 2D or 3D: the link between them disappears, the links to their common neighbours merge (here there is a total of five disappearances and two creations).

$\overline{\overline{T}}$ usually has only negative (resp. positive) eigenvalues. The variation in the number of sites and links is thus visible in the trace (sum of diagonal terms) of $\overline{\overline{T}}$.

When requested, all contributions of all topological changes can be treated indifferently and added together. This is certainly an advantage of the present description using matrices, over a classical counting as numbers (when counting the *number* of T1s and T2s, for instance, it would not make any sense to add them). In fact, some topological changes are significant, and do contribute to the pattern's evolution; while some changes are not physically relevant.

Consider the case where a topological change occurs between t and $t + \Delta t$, and the reverse one occurs between $t + \Delta t$ and $t + 2\Delta t$, so that the original links are recovered. This is often the case for neighbour exchanges, for instance due to thermal fluctuations; or, errors in the determination of links, in experiments or simulations, give rise to such pairs of opposite T1s, which are artifacts. Then the contributions to $\overline{\overline{T}}$ of both T1s are opposed and cancel each other, so that in average $\overline{\overline{T}}$ is not affected. Hence $\overline{\overline{T}}$ correctly describes the fact that the pattern is unchanged (while counting T1s as numbers would wrongly record 2 events) [4].

3 Statistical tools to obtain relative deformations and their time evolution

3.1 Continuous description

This section facilitates comparison between different experiments; or between experiments, simulations and theory. This is useful for flows of particle assemblies, in foams and emulsions, or granular materials. For biological tissues, it helps define the large scale flow (migration, rotation) during morphogenesis.

Here we try to link the discrete, local description with a continuous, global one. We want this continuous description to be self-consistent. For that purpose, we need to get rid of the discrete objects' length scale, that is, the typical size of links. We now construct tools which are dimensionless, or expressed in s^{-1} , but with no m^2 any longer. We thus construct a continuous counterpart $\overline{\overline{U}}$, $\overline{\overline{G}}$, $\overline{\overline{P}}$ for each of the three discrete quantities $\overline{\overline{M}}$, $\overline{\overline{C}}$, $\overline{\overline{T}}$ defined in section 2.

Averages $\langle \cdot \rangle$ on detailed geometrical quantities are performed on a spatial box of volume V_{box} and over a time τ selected to suit the problem under consideration.

$V_{box}\tau$ should be large enough, to include enough links to perform statistics, $N_{tot} \gg 1$. More precisely, $N_{tot}^{-1/2}$ should be smaller than the relative incertitude required by the user. A few tens or hundreds of links are often enough (there is no need for 10^{23} links!).

The shape of the box should preferably respect the system's symmetries. When there is a symmetry along one coordinate (for instance over time, for a steady state process [10], or over one space coordinate [12]), averaging over

this coordinate improves the statistics and enables to resolve better (average less) along other coordinates.

In particular, in the case of a steady flow, time averages on successive images can be performed. Thus it is enough to extract only a few links from each image: when multiplied by many images it yields a reasonably large N_{tot} . In this case V_{box} can be small enough to reflect physically relevant local variations. There is no theoretical lower limit to V_{box} : it can well be as small as the link size, or even smaller, if there are enough images to average (Fig. 6).

If the material acts as a continuous medium [21, 22, 23], it usually has the following properties. First, there exists a range of V_{box} sizes over which measurements yield the same results [14]. In that case, the box is called a representative volume element (RVE). This is usually obeyed if V_{box} is much larger than the range of interaction between individual objects, and also larger than their correlation length (but these conditions are neither necessary nor sufficient). Second, its description can be local in space, that is, its equation of evolution involves partial space derivatives, and the spatial variations of its solutions look smooth. Third, the average quantities have at large scale a role more important than that of fluctuations. The present paper is purely descriptive: it provides tools to investigate these aspects, but studying them in practical examples is the purpose of separate studies [15, 1].

3.2 Statistical internal strain : $\overline{\overline{U}}$

We first present the internal strain, defined through a comparison between the current pattern and a reference one. We provide more details than in the original reference by Aubouy *et al.* [9], hoping to make the reading easier.

3.2.1 Strain : from a single link to a pattern

Consider first a link ℓ of length ℓ , and apply to it an infinitesimal variation $d\ell$. Its relative extension, or infinitesimal strain, is $d\ell/\ell$, or equivalently $d(\log \ell)$ [24]. The "true strain" (also called "Hencky strain" [24]) is defined by with respect to a state ℓ_0 chosen as a reference (often a state without stress) using several equivalent expressions:

$$\begin{aligned} \int \frac{d\ell}{\ell} &= \log \left(\frac{\ell}{\ell_0} \right) \\ &= \frac{1}{2} \log \left(\frac{\ell^2}{\ell_0^2} \right) \\ &= \frac{1}{2} [\log(\ell^2) - \log(\ell_0^2)]. \end{aligned} \quad (14)$$

Here we have introduced ℓ^2 instead of ℓ (and compensated by a factor $1/2$). We also have replaced the log of division by a subtraction of log, which is strictly equivalent; it is not a problem to take the log of dimensioned quantities (here, the square of a length) because this cancels out in the final result.

We perform these manipulations because the last expression of eq. (14) is the easiest to generalise. We want to keep the information over the link orientation, as well as the statistical method to average over links. It is natural to replace ℓ^2 by the texture.

The logarithm of $\bar{\bar{M}}$ is unambiguously defined (section B.2) and is easily performed in three standard steps on a computer. It suffices to first, switch to the three orthogonal axes ($\bar{\bar{M}}$'s eigenvectors) in which $\bar{\bar{M}}$ is diagonal; second, take the logarithm of its eigenvalues, which are strictly positive (section 2.2.2):

$$\text{diag } \log \left(\bar{\bar{M}} \right) = \begin{pmatrix} \log \lambda_1 & 0 & 0 \\ 0 & \log \lambda_2 & 0 \\ 0 & 0 & \log \lambda_3 \end{pmatrix}; \quad (15)$$

and third, switch back to the original axes. It is necessary to perform first all linear operations such as averaging. This ensures in particular that all λ_i s in eq. (15) are non-zero. Taking the logarithm, which is a non-linear operation, has to be performed later.

Eq. (15), like eq. (14), requires to define a reference, expressed in the same units as $\bar{\bar{M}}$, so that the difference of their logarithms is well defined and dimensionless. Using a reference texture $\bar{\bar{M}}_0$, Aubouy *et al.* [9] thus define the ‘‘statistical internal strain’’ as:

$$\bar{\bar{U}} = \frac{1}{2} \left(\log \bar{\bar{M}} - \log \bar{\bar{M}}_0 \right). \quad (16)$$

Here $\bar{\bar{U}}$ completely characterises the material’s current deformation: relative dilation, amplitude and direction of anisotropy.

3.2.2 Reference texture $\bar{\bar{M}}_0$

This section is devoted to general comments regarding the reference texture $\bar{\bar{M}}_0$. Practical details are presented in appendix A.2.

Eq. (16) shows that the exact choice of $\bar{\bar{M}}_0$ affects the value of $\bar{\bar{U}}$ but not its variations. It thus does not appear explicitly in the kinematics (eqs. 65,23) nor in the dynamics (for instance in the value of the shear modulus, appendix A.3). Moreover, eq. (16) remains unchanged if we multiply both $\bar{\bar{M}}_0$ and $\bar{\bar{M}}$ by a prefactor; this is why the exact unit (*e.g.* m^2 , mm^2 , μm^2) in which $\bar{\bar{M}}_0$ and $\bar{\bar{M}}$ are expressed is unimportant, as long as it is the same unit for both.

Whatever the choice, the reference is defined by the texture $\bar{\bar{M}}_0$. It suffices to determine 6 numbers; or 3, in 2D; or 1, in the (most common) case where $\bar{\bar{M}}_0$ is isotropic. Only the reference texture corresponding to the current state matters; past changes of the reference pattern, for instance during an irreversible deformation (also called ‘‘work hardening’’ [23]), need not be taken into account.

It is never necessary to know the details of the corresponding pattern’s structure, such as the positions of each object one by one: it is even not necessary that this pattern exists and is realisable.

There are many different definitions of strain; see Refs. [25,12] for review. In particular, some definitions reflect accurately a discrete pattern’s geometry [26] or dynamics [27]. The main advantage of eq. (16) is that it does not require the detailed knowledge of each object’s past displacement. It is thus probably the only definition which extends much beyond the material’s elastic limit. It is valid even when bubbles rearrange and move past each other, that is, when the pattern flows.

3.2.3 Examples

This section presents a few examples and particular cases of internal strain.

(i) If the material is uniformly dilated (affine deformation, see section 4.1.2) by a factor k in all directions, then $\bar{\bar{M}} = k^2 \bar{\bar{M}}_0$. Thus $\bar{\bar{U}} = \log(k) \bar{\bar{I}}_D$, as is expected for instance for gases; that is, in 3D:

$$\bar{\bar{U}} = \begin{pmatrix} \log k & 0 & 0 \\ 0 & \log k & 0 \\ 0 & 0 & \log k \end{pmatrix}.$$

(ii) Conversely, if the material is uniformly dilated by a factor k in one direction and compressed by a factor $1/k$ in another direction, then:

$$\text{diag } \bar{\bar{U}} = \begin{pmatrix} \log k & 0 & 0 \\ 0 & -\log k & 0 \\ 0 & 0 & 0 \end{pmatrix}.$$

(iii) More generally, for incompressible materials, the links’ mean square length can vary, but $\bar{\bar{U}}$'s diagonal terms are usually both positive and negative, and their sum is certainly small. Then $\bar{\bar{U}}$ is mostly deviatoric (Appendix B.1).

(iv) In Fig. (9), most ellipses look circular; deviations from circles occur close to the obstacle (see also section 4.1.4). We distinguish regions where extension dominates, and ellipses look like coffee beans, from regions where compression dominates, where the ellipses are flattened. Up to a prefactor, namely the foam’s shear modulus, $(U_d)^2$ represents the elastic energy stored (that is, the difference between the energy of the current state and that of the local minimum) due to shear.

(v) If $\bar{\bar{M}}_0$ is isotropic, then $\bar{\bar{U}}$ is diagonal in the same axes as $\bar{\bar{M}}$. Then (15) enables to rewrite eq. (16) more explicitly:

$$\text{diag } \bar{\bar{U}} = \begin{pmatrix} \log \sqrt{\frac{\lambda_1}{\lambda_0}} & 0 & 0 \\ 0 & \log \sqrt{\frac{\lambda_2}{\lambda_0}} & 0 \\ 0 & 0 & \log \sqrt{\frac{\lambda_3}{\lambda_0}} \end{pmatrix}, \quad (17)$$

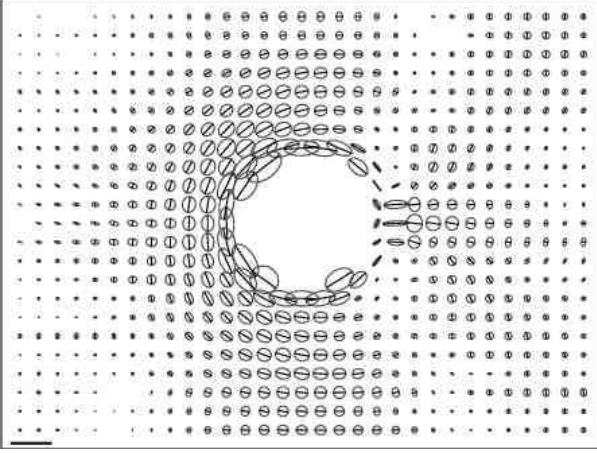


Fig. 9. Elastic behaviour. Map of the statistical internal strain \bar{U} (eq. 16) measured on the foam of Fig. (1a). Coffee bean axes indicate the direction and amplitude of stretching (indicated by a thin line) and compression. \bar{M}_0 is chosen as the value of \bar{M} measured at the left of the image, on each streamline, in order to be insensitive to a possible bubble size segregation. Scale: for ellipses, bar = 1 (dimensionless).

where λ_0 is \bar{M}_0 's eigenvalue (e.g. $\lambda_0 = \langle \ell_0^2 \rangle / 3$ is \bar{M}_0 if we use the definition of eq. 40). Eq. (17) reflects that \bar{M} and \bar{U} have the same eigenvectors: they commute. Eq. (17) also relates the trace of \bar{U} with \bar{M} 's determinant (product of eigenvalues):

$$\begin{aligned} \text{Tr } \bar{U} &= \log \sqrt{\frac{\lambda_1 \lambda_2 \lambda_3}{\lambda_0^3}} \\ &= \frac{1}{2} \log \left(\det \bar{M} \right) - \frac{1}{2} \log \left(\det \bar{M}_0 \right). \end{aligned} \quad (18)$$

(vi) in the limit of small deformations, *i.e.* when \bar{M} remains close enough to \bar{M}_0 , eq. (16) can be linearised [9]. The difference of logarithms would simply amount to a division by \bar{M}_0 , that is: $\bar{U} \simeq (\bar{M} - \bar{M}_0) \bar{M}_0^{-1} / 2$. This is true whether \bar{M}_0 is isotropic or not (unlike eq. 17). This approximation is used in Appendix C.2.2.

3.3 Kinematics: time evolution

3.3.1 Statistical velocity gradient: \bar{G}

We want to define the continuous counterpart of the geometrical changes \bar{C} (eq. 12). \bar{M}^{-1} (eq. 49), which is in m^{-2} , is always defined. We thus use it to define \bar{G} as:

$$\begin{aligned} \bar{G} &= \langle \ell \otimes \ell \rangle^{-1} \left\langle \ell \otimes \frac{d\ell}{dt} \right\rangle \\ &= \bar{M}^{-1} \bar{C}. \end{aligned} \quad (19)$$

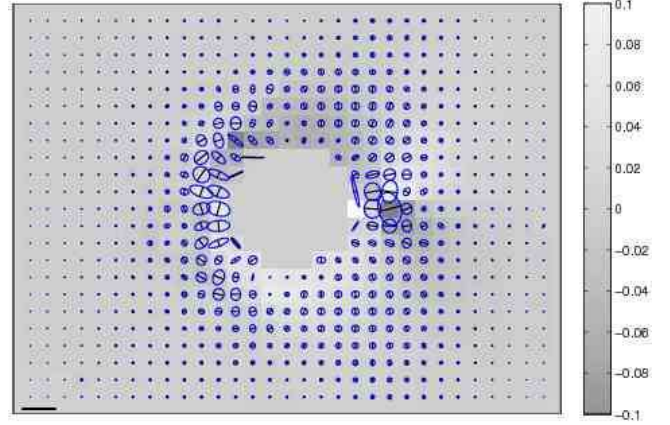


Fig. 10. Fluid behaviour. Map of the statistical symmetrised velocity gradient \bar{V} (eq. 20) measured on the foam of Fig. (1a). Coffee bean axes indicate the direction and amplitude of stretching rate (indicated by a thin line) and compression rate. Scale for ellipses: bar = 0.1 s⁻¹. Grey levels: statistical vorticity from the rotation rate $\bar{\Omega}$ (eq. 21) in s⁻¹.

\bar{G} has the dimension of a deformation rate (s⁻¹): its order of magnitude is the links' average variation rate. Like \bar{C} , it vanishes when the pattern moves as a whole ("solid translation").

For reasons which appear below (eqs. 29-31), we call it the "statistical velocity gradient", and we purposely define it as $\bar{M}^{-1} \bar{C}$ rather than $\bar{C} \bar{M}^{-1}$. In general, \bar{G} is not symmetrical.

In practice, the most useful quantity is its symmetric part, the "statistical symmetrised velocity gradient":

$$\bar{V} = \frac{\bar{G} + \bar{G}^t}{2} = \frac{\bar{M}^{-1} \bar{C} + \bar{C}^t \bar{M}^{-1}}{2}. \quad (20)$$

It is the rate of variation of \bar{M} due to the links' stretching and relaxation. Fig. (10) plots an example of \bar{V} . It is large all around the obstacle, but only very close to it; it is almost symmetrical before and after the obstacle. When the material's density is constant, $\text{Tr} \bar{V}$ is small, and the corresponding ellipse is nearly circular.

The anti-symmetric part is the statistical rotation rate:

$$\bar{\Omega} = \frac{\bar{G} - \bar{G}^t}{2} = \frac{\bar{M}^{-1} \bar{C} - \bar{C}^t \bar{M}^{-1}}{2}. \quad (21)$$

It has 3 independent components in 3D, but only 1 in 2D (appendix B.1). Thus Fig. (10) plots it as grey levels.

3.3.2 Statistical topological rearrangement rate: \bar{P}

We define the continuous counterpart of the topological changes \bar{T} (eq. 13) in a way similar to section (3.3.1). Since

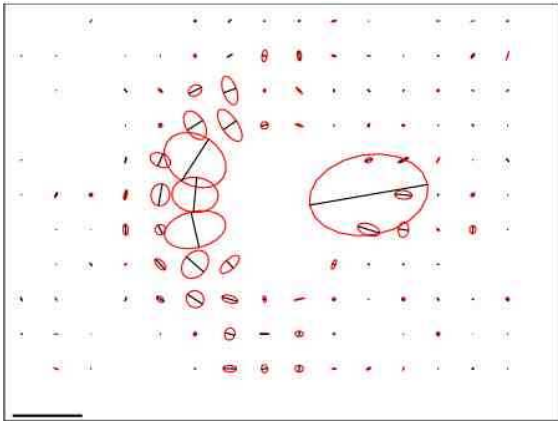


Fig. 11. Plastic behaviour. Map of the topological deformation rate $\bar{\bar{P}}$ (eq. 22) measured on the foam of Fig. (1a). Coffee bean axes indicate the direction of links which have just disappeared (indicated by a thin line) and just appeared; note that this is the inverse of Fig. (8), due to the minus sign in eq. (22). Scale for ellipses: bar = 0.1 s^{-1} , proportional to the frequency of rearrangements. Measurement boxes touching the obstacle were removed.

$\bar{\bar{T}}$ is symmetric, we suggest to construct its counterpart $\bar{\bar{P}}$ directly as symmetric too, as in eq. (20):

$$\bar{\bar{P}} = -\frac{1}{2} \frac{\bar{\bar{T}}\bar{\bar{M}}^{-1} + \bar{\bar{M}}^{-1}\bar{\bar{T}}}{2}. \quad (22)$$

Here we have introduced a factor $-1/2$ so that $\bar{\bar{P}}$ is the term which unloads the statistical internal strain, as will appear in eqs. (65,23). In cases where $\bar{\bar{T}}$ and $\bar{\bar{M}}$ commute, such as in the companion paper [15], $\bar{\bar{T}}\bar{\bar{M}}^{-1}$ is symmetric and eq. (22) simply writes $\bar{\bar{P}} = -\bar{\bar{T}}\bar{\bar{M}}^{-1}/2$.

This “statistical topological rearrangement rate” $\bar{\bar{P}}$ (eq. 22) has the dimension of s^{-1} . It measures the frequency and direction of rearrangements: it is of the order of magnitude of the number of changes per unit time and per link. Corresponding coffee beans are elongated (resp: flattened) if the number of links decreases (resp: increases); if the number of links is conserved, coffee beans are nearly circular.

As an example, Fig. (11) shows that the rearrangements are more frequent just in front of the obstacle, or in a very narrow region behind it. The rate of rearrangements decreases smoothly with the distance to the obstacle. This is due to the foam’s elasticity. It contrasts with the sharp transition between solid-like and fluid-like regions observed in purely visco-plastic materials [28,29]. Note that, since there are only few topological events, the size of boxes has been chosen large (same as Fig. 6a), to keep reasonable statistics. The companion paper [15] presents an example with a larger spatial distribution of topological events, which enables for a better spatial resolution.

3.3.3 Kinematic equation of evolution

We have thus three independent symmetric matrices: $\bar{\bar{U}}$, $\bar{\bar{V}}$ and $\bar{\bar{P}}$. As discussed in Appendix C.2.3, there is a relation between them. In the case where we can neglect $\bar{\bar{M}}$ ’s advection and rotation, its time evolution (eq. 10) approximately simplifies as:

$$\bar{\bar{V}} = \frac{\mathcal{D}\bar{\bar{U}}}{Dt} + \bar{\bar{P}}. \quad (23)$$

That is, the (statistical) symmetrised velocity gradient is shared between two contributions: one part changes the (statistical) internal strain, the other part is the (statistical) topological rearrangement rate. How $\bar{\bar{V}}$ is shared between both contributions constitutes the main subject of the companion paper [15].

Physically, eq. (23) means that, when a perturbation is applied to the overall shape of the pattern, part of it affects the appearance of the pattern (loading) and the other part goes into rearrangements (unloading). Section 4 introduces a parallel point of view, in particular with eq. (27).

4 Mechanics

This section, which addresses applications of our tools beyond the simple description, is more theoretical.

In the section 3, we have introduced statistical measurements based on discrete objects. They describe the pattern’s connections (topology), shape (geometry) and movements (kinematics). On the other hand, continuous mechanics describes forces (or stresses), that is, dynamics. A given region of the pattern is said to be in elastic, plastic or viscous (or fluid) regime, according to the contribution to the stress that dominates locally [30]. The viscous (or fluid) contribution to stress is irreversible: it is due to, and thus increases with, the velocity gradient; that is, relative movements of objects within the material. The elastic contribution to stress is reversible, while the plastic one is irreversible; both are solid behaviours, that is, exist in the limit of very low velocity gradient.

In order to unify the description of the three regimes, we would like to identify the statistical and dynamical descriptions. We first recall that continuous mechanics involves three kinematical quantities $\dot{\bar{\bar{\epsilon}}}_{tot}$, $\dot{\bar{\bar{\epsilon}}}_{el}$ and $\dot{\bar{\bar{\epsilon}}}_{pl}$ (section 4.1.1), which are related through eq. (27). We then try to identify it with eq. (23). This is possible, not in general, but in particular cases.

We thus proceed step by step. Section 4.2 shows that in affine deformations we can approximately identify $\bar{\bar{V}}$ and $\dot{\bar{\bar{\epsilon}}}_{tot}$. To proceed further, section 4.1.2 considers the case where either $\mathcal{D}\bar{\bar{\epsilon}}_{el}/Dt$ or $\dot{\bar{\bar{\epsilon}}}_{pl}$ vanishes, and thus the number of independent quantities reduces to 1; section 4.3.2 investigates the case of foams. We hope that in these cases, statistical measurements can constitute a coherent

language to unify the description of elastic, plastic and fluid behaviours, as well as facilitate models and tests.

4.1 Link with continuous mechanics

4.1.1 Elastic, plastic, fluid behaviours

If the pattern behaves as a continuous material, we can consider a representative volume element, or RVE (section 3.1). If this RVE is at position \mathbf{R} , the velocity field is $\langle \mathbf{v} \rangle (\mathbf{R})$, that is, an average over the whole RVE. If \mathbf{R}_1 and \mathbf{R}_2 are the positions of two RVEs, the velocity gradient $\overline{\nabla v}$ is the spatial derivative of the velocity field, and $\overline{\nabla v}^t$ is its transposed (eqs. 52,53), then:

$$\langle \mathbf{v} \rangle (\mathbf{R}_2) \simeq \langle \mathbf{v} \rangle (\mathbf{R}_1) + \overline{\nabla v}^t \cdot (\mathbf{R}_2 - \mathbf{R}_1). \quad (24)$$

Details on this notation can be found in Appendix B.3. Eq. (24) neglects terms of order of $|\mathbf{R}_2 - \mathbf{R}_1|^2$ and higher. It describes the velocity field as continuous and affine, that is, a term which varies linearly with position plus a constant.

One of the key ingredients of continuous mechanics is the velocity gradient's symmetrical part, that is, the total deformation rate:

$$\dot{\overline{\varepsilon}}_{tot} = \frac{\overline{\nabla v} + \overline{\nabla v}^t}{2}. \quad (25)$$

This is a purely kinematical quantity, but it determines the contribution to the viscous (dissipative) stress [21].

For small deformations (linear regime), neglecting advection and rotation, the integration of eq. (25) defines a total applied deformation, which is a function of the past history of the sample, as:

$$\overline{\varepsilon}_{tot} = \int dt \dot{\overline{\varepsilon}}_{tot} \approx \frac{\overline{\nabla u} + \overline{\nabla u}^t}{2}. \quad (26)$$

Here $\overline{\nabla u}$ is the gradient of the displacement field \mathbf{u} , and $\overline{\varepsilon}_{tot}$ its symmetrical part.

The total deformation rate contributes in part (loading) to change the elastic strain $\overline{\varepsilon}_{el}$, and in part (unloading) to a plastic deformation rate $\overline{\varepsilon}_{pl}$ which is defined by:

$$\dot{\overline{\varepsilon}}_{tot} = \frac{\mathcal{D} \overline{\varepsilon}_{el}}{\mathcal{D}t} + \dot{\overline{\varepsilon}}_{pl}. \quad (27)$$

Both are defined through dynamics. The elastic strain $\overline{\varepsilon}_{el}$ contributes to the reversible part of the stress. The plastic strain rate $\dot{\overline{\varepsilon}}_{pl}$ describes the irreversible contribution to the stress in the low velocity limit (note that rearranging patterns can often deform a lot without breaking).

4.1.2 Affine assumption

The *affine assumption* is analogous to, but much stronger than, eq. (24). It assumes that the velocity of *each* individual object is affine too:

$$\mathbf{v}(\mathbf{r}_2) \stackrel{\text{affine}}{\simeq} \mathbf{v}(\mathbf{r}_1) + \overline{\nabla v}^t \cdot (\mathbf{r}_2 - \mathbf{r}_1). \quad (28)$$

In other words, it assumes that the continuous velocity gradient has a meaning down to the level of individual objects, and that fluctuations around it are small enough to have no effect on the material's mechanical behaviour.

In cellular patterns, especially in dry ones where there are no gaps nor overlaps, the movement of each individual object is highly correlated with its neighbours'. Thus the affine assumption is reasonable, see section 4.1.4 and in particular Fig. (12). In particle assemblies, it might apply to dense assemblies of repelling particles, which cannot be too close nor too far from each other. Whenever this assumption is valid, it considerably simplifies the description of the pattern evolution.

Consider for instance a link, $\ell = \mathbf{r}_2 - \mathbf{r}_1$ (eq. 1). Its time derivative is

$$\frac{d\ell}{dt} = \mathbf{v}(\mathbf{r}_2) - \mathbf{v}(\mathbf{r}_1).$$

Thus, under the affine assumption (eq. 28), the velocity gradient modifies all links in almost the same way by (see eq. 54):

$$\frac{d\ell}{dt} \stackrel{\text{affine}}{\simeq} \overline{\nabla v}^t \ell. \quad (29)$$

In the definition (eq. 12) of \overline{C}^t , the velocity gradient can be taken out of the average:

$$\begin{aligned} \overline{C}^t &\stackrel{\text{affine}}{\simeq} \left\langle \overline{\nabla v}^t \ell \otimes \ell \right\rangle \\ &= \overline{\nabla v}^t \langle \ell \otimes \ell \rangle. \end{aligned} \quad (30)$$

By injecting eq. (30) into eq. (19) we show that \overline{G} is a statistical equivalent of the velocity gradient $\overline{\nabla v}$:

$$\overline{G} = \overline{M}^{-1} \overline{C} \stackrel{\text{affine}}{\simeq} \overline{\nabla v}. \quad (31)$$

This is why we included \overline{M}^{-1} only on the right side of \overline{G} (eq. 19).

In a deformation at constant volume, $\overline{\nabla v}$ has a zero trace, so \overline{G} approximately has a zero trace too.

4.1.3 Velocity gradient and total deformation rate

By comparing eq. (25) with eqs. (20,31) we identify the statistical and dynamical definitions of the total deformation rate:

$$\overline{V} \stackrel{\text{affine}}{\simeq} \dot{\overline{\varepsilon}}_{tot}. \quad (32)$$

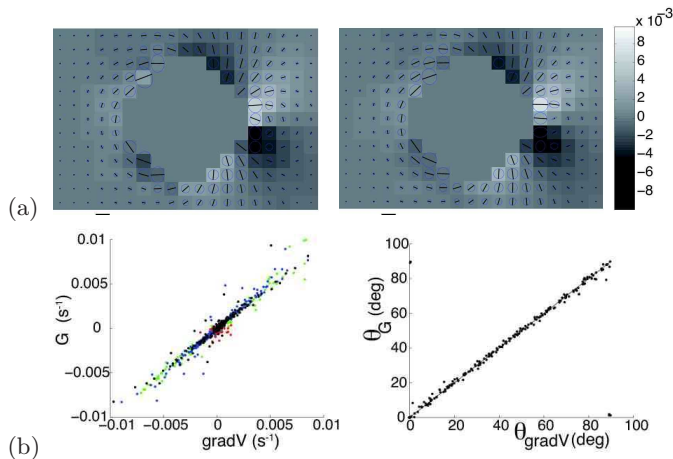


Fig. 12. Affine assumption: test of eq. (31) on a foam. (a) Comparison of maps of \overline{G} (left) and $\overline{\nabla v}$ (right): ellipses, symmetric part; grey levels, antisymmetric part (bar: $5.6 \times 10^{-3} \text{ s}^{-1}$). (b) Quantitative comparison: left, $(G_{XX} - G_{YY})/2$ versus $(\nabla v_{XX} - \nabla v_{YY})/2$, and the same for all other components (superimposed): $XX + YY$, $XY - YX$, $XY + YX$; right, angle (in degrees) of ellipses plotted in (a). Each point comes from one RVE of the image.

\overline{V} thus appears as a statistical measurement of the symmetrised velocity gradient $\overline{\dot{\varepsilon}}_{tot}$. When only large scale measurements are possible, only $\overline{\dot{\varepsilon}}_{tot}$ can be measured. However, when the detailed information on links is available to perform statistics, measuring \overline{V} offers several advantages.

First, the signal to noise ratio is optimal, in the sense that all the local information, and only it, is used.

Moreover, \overline{V} is intrinsically based on the material's structure. It can be defined and measured even if there are only a few objects or if the standard deviation of their velocities is large. Each link acts as a small probe of the local velocity differences: the spatial derivative is taken naturally at the places where the objects are, not on a large scale lattice of RVEs. Averaging over all links provides a statistical measurement of the continuous deformation rate. At no point does the definition or measurement of \overline{V} require any affine description.

Physically, we expect \overline{V} to play a more general role than $\overline{\dot{\varepsilon}}_{tot}$, because it is based on the individual objects themselves. For instance, we expect \overline{V} to be determinant in yielding, and thus in the description of plasticity (and possibly $\overline{\Omega}$ too) [15]. Similarly, the material's internal dissipations are probably more closely related to changes in the links than to a large scale velocity gradient: this suggests that the dissipative contribution to the stress arises in general from \overline{V} rather than from $\overline{\dot{\varepsilon}}_{tot}$.

4.1.4 Example

Using our example of foam, we have checked eq. (31) at different scales (the same as in Fig. 6). Fig. (12) shows some of our measurements. We have measured the detailed components, including the rotational (asymmetric part), as well as eigenvalues and axes of the symmetric part.

All these quantities are the same for \overline{G} and $\overline{\nabla v}$, within a few percents precision, with a correlation close to 1. The measurements of \overline{G} and $\overline{\nabla v}$ have a comparable precision, and suffer from similar imprecisions near the channel walls and obstacle. Both have a small trace (ellipses are nearly circular), see section 3.2.3.

This agreement is unexpectedly good, given that with the dry foam chosen here the deformation is large and its gradient is strong. At large scale, movements of individual objects within the same RVE can differ considerably; but even in this unfavorable case, the affine assumption seems to hold, as shown in Fig. (12). The reason seems to be that eq. (31) is correct whenever \overline{M} does not vary significantly within the chosen RVE [1].

4.2 Identification of matrices under the affine assumption

4.2.1 Strain, in the elastic regime

In this section we consider the particular case where the material is in the elastic regime; first, for simplicity, the linear elastic regime; then back to the general one.

In elastic regime, there is no plastic deformation rate, $\overline{\dot{\varepsilon}}_{pl} = 0$. Eq. (27) becomes simply:

$$\frac{D \overline{\varepsilon}_{el}}{Dt} = \overline{\dot{\varepsilon}}_{tot}. \quad (33)$$

Thus, in the elastic regime, the elastic strain and the deformation rate are not independent physical quantities. Combining eqs. (26) and (33) shows that $\overline{\varepsilon}_{el} \approx \overline{\varepsilon}_{tot}$. That is, in the linear elastic regime, one can identify two quantities: the symmetrised gradient of the displacement field, $\overline{\varepsilon}_{tot}$, which is a function of the past history of the sample; and the elastic strain $\overline{\varepsilon}_{el}$, which is a function of state. In fact, in elasticity, both quantities are considered as equivalent [22].

On the other hand, under the affine hypothesis, Ref. [9] for the linear elastic regime (small deformations), and Ref. [12] for the non-linear elastic regime (large deformations), show that:

$$\overline{U}^{\text{affine elastic}} \approx \overline{\varepsilon}_{tot}. \quad (34)$$

The demonstration of eq. (34) is similar to that for \overline{V} (eqs. 30-32): it uses the same hypotheses, with the additional assumption that \overline{M} and \overline{M}_0 commute (which is satisfied if \overline{M}_0 is isotropic).

Eq. (34) shows that in the elastic regime $\bar{U} \approx \bar{\varepsilon}_{el}$. Thus the elastic strain $\bar{\varepsilon}_{el}$ can be measured using two different methods. When large scale measurements of total deformation are possible, $\bar{\varepsilon}_{el}$ can be measured as $\bar{\varepsilon}_{tot}$. When the detailed information on links is available, measuring $\bar{\varepsilon}_{el}$ as \bar{U} offers many advantages, similar to that of \bar{V} (section 4.1.3).

4.2.2 Plastic deformation rate, in steady flow

In the more general case, there is a plastic deformation rate, $\dot{\bar{\varepsilon}}_{pl} \neq 0$, and deformations can be non affine. Eq. (33) does not hold. The current elastic strain $\bar{\varepsilon}_{el}$ and the total deformation rate $\dot{\bar{\varepsilon}}_{tot}$ are independent physical quantities; $\bar{\varepsilon}_{el}$ can no longer be measured as $\bar{\varepsilon}_{tot}$. Whether it can be measured as \bar{U} is discussed in section 4.3.

For instance, if the material flows, involving arbitrary large displacements, $\dot{\bar{\varepsilon}}_{pl}$ can become much larger than $\mathcal{D} \bar{\varepsilon}_{el} / \mathcal{D}t$. In the extreme cases of steady flows, independent of time, it is possible (in absence of advection) that $\mathcal{D} \bar{\varepsilon}_{el} / \mathcal{D}t = 0$, and eq. (27) reduces to:

$$\dot{\bar{\varepsilon}}_{tot} = \dot{\bar{\varepsilon}}_{pl}. \quad (35)$$

According to eq. (22), a steady flow with a corotational derivative that vanishes (meaning no advection nor rotation effects, see eq. (66)), implies that all the geometrical deformation rate translates into the topological deformation rate:

$$\bar{P} = \bar{V}.$$

Using the identification of eq. (32), we therefore obtain in that case:

$$\bar{P} \stackrel{\text{affine}}{\underset{\text{steady}}{\simeq}} \dot{\bar{\varepsilon}}_{pl}. \quad (36)$$

4.3 Complete identification

4.3.1 General case

The statistical tools \bar{U} and \bar{P} are always defined and measurable, even out of the elastic regime or out of the steady regime. If we could identify them with $\bar{\varepsilon}_{el}$ and $\dot{\bar{\varepsilon}}_{pl}$, respectively, it would make possible to measure the elastic strain in all regimes. This is certainly not possible in general, as shown by the following counterexamples [31].

In granular systems, due to solid friction in the contacts, irreversible plastic strains appear before the list of contacts changes. In solid networks (*e.g. solid foams*) with no topological change, the bond themselves might behave plastically, or they might perhaps undergo buckling instabilities leading to non-reversible stress-strain curves. Those are examples in which plasticity occurs *before* the first topological change.

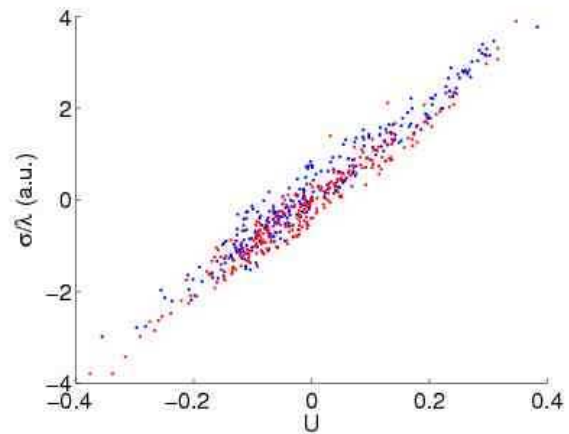


Fig. 13. XY components of the elastic stress σ (in arbitrary units) versus XY components of \bar{U} . Each point comes from one RVE of the image. Data for the $(XX - YY)/2$ components are superimposed. For details of the measurement method see refs. [11, 10, 12].

Conversely, consider a set of rigid cables which resist tension, but no compression, and tie them together at knots to form a redundant, hyperstatic network. Under given external forces on the knots, some cables will be taut, others will dangle and transmit no force. Upon changing the forces, the list of taut, tension-carrying cables will change. This can be regarded as a topological change. The response, which implies displacements and strains, is however reversible and might be called elastic. Hence a case for which plasticity begins *after* the first topological change.

4.3.2 The case of foams

Identification is apparently possible in at least one case, that of liquid foams (or emulsions). As we have seen in section 4.1.4, they obey the affine hypothesis, as probably do many cellular patterns. This is already an important property; see also the discussion in Appendix A.3. However, they have two additional properties, which are very specific.

Firstly, in a foam, the elastic energy is proportional to the bubble surfaces, so that the elastic strain stems from bubble deformation. This has been experimentally checked: \bar{U} (or at least its deviatoric part) actually determines the (deviatoric) elastic stress [11, 10, 12]. Their proportionality factor is a measurement of the shear modulus. We check it on our example too (Fig. 13).

Secondly, each topological process instantaneously changes the energy landscape, leading to a relaxation within a new attraction basin, and thus an irreversible plastic change [15]. There is thus a direct link between the discrete pattern and its continuous mechanical behaviour. This suggests that it should be possible to achieve the identification:

$$\bar{U} \stackrel{\text{foams}}{\simeq} \bar{\varepsilon}_{el},$$

$$\begin{aligned}\bar{P} &\simeq \dot{\bar{\varepsilon}}_{pl}, \\ \bar{V} &\simeq \dot{\bar{\varepsilon}}_{tot}.\end{aligned}\quad (37)$$

5 Summary

In the present paper, we define tools (Table 1) to extract information from a pattern made of discrete objects, subject to rearrangements, within a wide class of complex materials made of individual constituents such as atoms, molecules, bubbles, droplets, cells or solid particles. They characterise quantitatively the mutual arrangements of these objects, or more precisely the links between neighbouring objects.

Their definition, which can flexibly adapt to the questions to be answered, is operational. That is, given an experimental or simulated pattern, whether in 2D or 3D, there is a well defined method to measure them directly as statistics on individual constituents (links between neighbouring sites). This measurement is easy, and requires only a few basic operations on a computer: multiplication, average, diagonalisation, logarithm. It is robust to experimental noise, even if there is a limited number of links.

\bar{M} , \bar{C} and \bar{T} characterise the current state of the pattern, its geometrical changes, and its topological rearrangements, respectively. They are explicitly based on the pattern's discrete structure. They can be measured locally, for instance on a single biological cell, or grain in crystals. But they can also be measured as averages over a larger region in space, or as time averages.

For instance, in foams, measuring them smoothens out the pattern fluctuations due to the discrete nature of bubbles, and evidences the underlying behaviour of the foam as a continuous medium.

Their statistical counterparts, \bar{U} , \bar{G} (or rather \bar{V}) and \bar{P} , are independent of the pattern's discrete length scale. Each of them exists and is valid together in elastic, plastic and fluid regimes : they unify the description of these three mechanical behaviours. It facilitates the comparison between experiments, simulations and theories.

In at least two cases: (i) linear, affine, elastic regime; and (ii) foam mechanics, we suggest how to identify them with the quantities which characterise the continuous mechanics: elastic strain, total deformation rate, and plastic deformation rate, respectively. From a practical point of view, this offers the advantage of measuring these continuous quantities with an optimal signal to noise ratio, even with few discrete objects. On a fundamental side, this provides a physical basis to the description of a continuous medium, at any local or global scale, by relating it to the individual constituents. Moreover, it provides a coherent language common to elasticity, plasticity and fluid mechanics.

The companion paper [15] illustrates most of these points on a detailed practical example.

Acknowledgments

This work was initially stimulated by a seminar delivered by G. Porte. We thank M. Aubouy, S. Courty, J.A. Glazier, E. Janiaud, V. Grieneisen, Y. Jiang, J. Käfer, S. Marée for discussions. We thank the colleagues who have made constructive comments about the first version of the manuscript.

A Measurement techniques

This Appendix, aimed at non-specialists, lists practical advices based on our past experience.

A.1 Averaging procedure

There are at least three main possible choices for the averaging procedure (Fig. 14). Once a procedure has been selected, it is important to keep consistently the same for all measurements.

The *topology* is useful for local information, typically to measure \bar{M} or \bar{T} for a single particle or cell. This is the case for instance when studying the division of a cell [4]. In that case, each link is either included or excluded (“all or nothing”). One should at least include the links between the site of interest and its neighbours (first shell). One can also choose to include the second shell (next nearest neighbours), third, or even higher. Statistics are over a few links only, and are easy to compute, even sometimes by hand.

The *geometry* is useful for a continuous description, typically to measure $\bar{U}(\mathbf{R}, t)$, $\bar{P}(\mathbf{R}, t)$ or $\bar{V}(\mathbf{R}, t)$ in a RVE as a function of space and time. This is the case for the examples of foam flow which illustrate this paper. The average is over all links in a box which respects as much as possible the symmetry of the problem: rectangle, annulus. The dimensions of the box determine the scale of averaging. The measurements are performed on boxes at different positions \mathbf{R} . The distance between measurements positions cannot be more distant than the box size (it would leave gaps between boxes), but they can be closer (thus boxes overlap). If the box dimension is much larger than a link, one might choose to neglect links which cross the box boundary. But in general, links which cross the boundary require attention (especially near the box corner) if an automatised image analysis is used. An additional choice is required. A first possibility (“all or nothing”), computationally simpler, is to look where the link's center lies: if the center lies inside the box, the link is assigned to this box; else, this link is not counted [10] or assigned to this box with a weight 1/2 [14]. A second possibility (“proportional”), which yields a better precision, consists in determining the fraction w of the link which is inside the box (the remaining $1 - w$ is outside); then the link is counted in the statistics with a weight w [12], see also Appendix C.1.

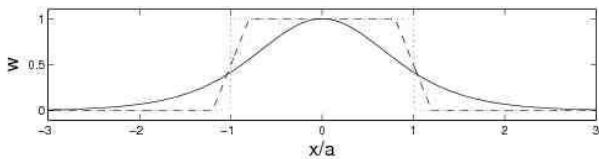


Fig. 14. Examples of averaging procedures: a link’s weigh w vs its position, here the box range is the segment $[-a, a]$. Dots: “all or nothing”. Dashes: “proportional”. Solid line: “coarse grained”, here with a hyperbolic tangent profile.

The *coarse graining* is seldom convenient in the practical applications considered here. However, specialists use it for theory [27], especially for the advection term (see Appendix C.1) [17]. A link at position \mathbf{r} is counted in a box at position \mathbf{R} with a weight $w(|\mathbf{r} - \mathbf{R}|)$. The coarse graining function w is a function which is non-increasing, from $w(0) = 1$ to $w = 0$, and has an integral equal to 1. Its width at half height (that is, where $w = 1/2$) defines the scale of coarse graining. It is a continuous and differentiable function, so that advected links enter and leave the average smoothly, without singularity [27].

Once the procedure has been chosen, we note:

$$N_{tot} = \sum w,$$

where the sum is taken over all links in the averaging region; and the average of any quantity x is:

$$\langle x \rangle = N_{tot}^{-1} \sum w x.$$

For instance, the texture is:

$$\bar{M} = \langle \ell \otimes \ell \rangle = \frac{\sum w \ell \otimes \ell}{\sum w} \quad (38)$$

There are other details which we have not tested yet. For instance, regarding particles or cells placed at the pattern’s boundary. Or for images of low quality (for instance due to defocalisation in 3D patterns, or low contrast), in which particles or cells are difficult to identify. We encourage the user to develop and test specific procedures, and if possible to keep us informed.

A.2 Choice of \bar{M}_0

Since the reference texture \bar{M}_0 plays almost no physical role, its choice is not very important. It depends on the problem under consideration, but once its definition is chosen, it should be kept consistently. We now list a few possibilities, with decreasing available information.

The most favorable case is when \bar{M}_0 can be measured directly. In experiment, this is possible when an image can be chosen as reference, for instance a stress free pattern. In simulation (Fig. 3b), this requires to relax the stress under prescribed constraints.

In theory, \bar{M}_0 can be determined in a set of particles with known interaction potential; for instance in Fig. (3a),

where the natural reference is the honeycomb pattern with a link size:

$$\ell_0^2 = \frac{2A}{\sqrt{3}} = 2\sqrt{3}A_{link}. \quad (39)$$

Here A is the area per particle (or cell), $A_{link} = A/3$ is the area per link, and $\bar{M}_0 = \ell_0^2 \bar{I}_2 / 2$.

In many cases (Fig. 1), no reference state is known in details. If only $\langle \ell_0^2 \rangle$ is known, we suggest to take \bar{M}_0 as isotropic. Although we don’t know any fundamental reason for that, it seems to be satisfactory in all practical cases we have encountered. From eqs. (5, 8) it writes, in $D = 2$ or 3 dimensions:

$$\bar{M}_0 = \frac{\langle \ell_0^2 \rangle}{D} \bar{I}_D, \quad (40)$$

In some cases, $\langle \ell_0^2 \rangle$ is not known but we can estimate it. For instance, in a 2D cellular pattern of known average area $\langle A \rangle$ (Fig. 2), the comparison with hexagons (eq. 39) suggests to take approximately :

$$\langle \ell_0^2 \rangle \approx \frac{2\langle A \rangle}{\sqrt{3}}, \quad (41)$$

In the worst case, even $\langle \ell_0^2 \rangle$ is unknown. A possibility is to take:

$$\bar{M}_0 \approx \bar{\lambda} \bar{I}_D,$$

where $\bar{\lambda}$ is the average of the λ_i s, \bar{M} ’s eigenvalues. Taking the arithmetic average, $\bar{\lambda} = \sum_i \lambda_i / D$, corresponds to the assumption that $\langle \ell^2 \rangle$ is conserved: $\langle \ell_0^2 \rangle \approx \langle \ell^2 \rangle$. Taking the geometric average, $\bar{\lambda} = (\prod_i \lambda_i)^{1/D}$, corresponds to the assumption that $\text{Tr} \bar{U} = 0$, which is close to assuming that the material is incompressible (see section 3.2.3).

A.3 The case of cellular patterns, especially foams

In dry cellular patterns, the number of neighbours of each cell is variable; but its average over the whole pattern is always close to 6 neighbours, and thus 6 links, per cell [18, 16]. Since each link is shared by two cells, the number of links is 3 times the number of cells. This is also true for a moderately wet cellular pattern, if neighbours are defined on a skeletonized image. It extends to Voronoi/Delaunay definition of neighbours for particles.

Aubouy *et al.* [9] chose to describe a cellular pattern such a 2D dry foam as a network, each site being a vertex (that is, a point where three cells meet). Here, we prefer to use cell centers, for several reasons. (i) First, and most important: the centers move according to the overall velocity field (while vertices have a highly fluctuating displacement), thus the affine assumption (eq. 28) applies. (ii) It is more robust, because a cell center is measured as an average over several pixels (while a vertex is a single pixel, which position might depend on the image analysis procedure). (iii) This has the advantage of being more general: it applies to all other discrete patterns; and even within cellular patterns, it applies to wet foams, and to

3D. (iv) Finally, the topological rearrangements are well characterised (while on the opposite, if ℓ was defined as the vector between two vertices, a T1 occurs would be defined as $\ell_a = \ell_d = 0$, so that the contribution of a T1 to eq. 13 would systematically be zero!).

Marée *et al.* [32] propose to measure the shear modulus by considering the variation of cell shapes. Each cell's shape is characterised by its inertia matrix: it looks similar to eq. (2), but it is averaged over the pixels inside a cell; thus their description is *intra-cellular*. Ours, averaged over the links between the cells, and thus based on the shape of the overall pattern, is rather *inter-cellular*. In dry cellular patterns, where there are no gaps between cells, nor overlaps, the deformation of each cell is highly correlated to the global deformation; thus, in this case, both descriptions coincide and yield approximately the same results [4]. Here, we prefer to use the texture based on cell centers, which is more general, for several reasons. (i) It also applies to characterise the deformation of wet foams (where bubbles are round, and thus each bubble's inertia is isotropic). (ii) It applies to all other discrete patterns, including particle assemblies. (iii) Centers, rather than shape, are involved in the kinematic description, including eqs. (20,22).

Finally, note that the shear modulus is the variation of elastic stress with respect to infinitesimal variations of \bar{U} . This measurement is robust [11,10,12]. As mentioned in section 3.2.2, it is not affected if we multiply \bar{M} and \bar{M}_0 by a same prefactor; and even if we change \bar{M}_0 , see for instance eq. (16). This is why this particular measurement gives similar results with both above methods.

B Matrices: notations and definitions

We work here in a space with $D = 3$ dimensions, although many practical applications regard 2D images. A *scalar* is a simple number; a *vector* is a list of D numbers, and we note it with an arrow; a *matrix* is an array of $D \times D$ numbers, and we note it with a double bar. All these objects are *tensors*, of rank 0, 1 and 2, respectively. Tensors of rank 3, for which there exist no particular name, are barely used in the present paper, and we note it with a triple bar.

This appendix is aimed at readers who are not familiar with the matrices. We thus list all relevant definitions used in the text, from the simplest to the most complicated, but all of them are standard.

B.1 Notations and definitions

Throughout this paper we manipulate matrices using a compact notation for simplicity. In this Appendix we use a developed notation, easier to understand, using components (labelled by 2 indices) rather than double bar. Both notations are equivalent; both ensure that the equations we write are independent of the system of axes we choose.

A matrix \bar{A} is an array with components A_{ij} , where $i, j = 1, 2$ or 3 :

$$\bar{A} = \begin{pmatrix} A_{11} & A_{12} & A_{13} \\ A_{21} & A_{22} & A_{23} \\ A_{31} & A_{32} & A_{33} \end{pmatrix}. \quad (42)$$

Its *trace* is the sum of its diagonal terms:

$$\text{Tr } \bar{A} = A_{11} + A_{22} + A_{33}. \quad (43)$$

Its *transposed* \bar{A}^t has components $A_{ij}^t = A_{ji}$, and has the same trace. Any matrix can be rewritten as the sum of its *symmetric* and *antisymmetric* parts:

$$\bar{A} = \frac{\bar{A} + \bar{A}^t}{2} + \frac{\bar{A} - \bar{A}^t}{2}.$$

A matrix \bar{S} is said to be *symmetric* if it is equal to its transposed, $\bar{S} = \bar{S}^t$ (while an antisymmetric matrix is equal to minus its transposed); by definition, the symmetric part of \bar{A} is always symmetric. A symmetric matrix can itself be rewritten as an isotropic term and a traceless (or *deviatoric*) term:

$$\bar{S} = \frac{\text{Tr}(\bar{S})}{D} \bar{I}_D + \text{Dev}(\bar{S}), \quad (44)$$

where \bar{I}_D is the identity matrix in dimension D (eq. 5), and:

$$\text{Dev}(\bar{S}) = \bar{S} - \frac{\text{Tr}(\bar{S})}{D} \bar{I}_D. \quad (45)$$

Itself, the deviatoric part can be decomposed in diagonal components, called *normal differences*, and off-diagonal ones.

To summarize, a matrix has in general 9 independent components A_{ij} . They can be rewritten as 3 antisymmetric ones, namely $(A_{12} - A_{21})/2$, $(A_{23} - A_{32})/2$, and $(A_{31} - A_{13})/2$; and 6 symmetric ones, namely 1 trace $A_{11} + A_{22} + A_{33}$, 2 normal differences $A_{11} - A_{22}$ and $A_{22} - A_{33}$, 3 off-diagonal terms $(A_{12} + A_{21})/2$, $(A_{23} + A_{32})/2$, and $(A_{31} + A_{13})/2$. This means that an antisymmetric matrix has 3 independent components, a symmetric matrix has 6, a deviatoric one has 5, an isotropic one has 1.

Tensorial notations are valid in any dimension D , and it is straightforward to rewrite them in 2D, see also section 2.2.3. In 2D, a matrix \bar{A} has in general 4 independent components A_{ij} , where $i, j = 1$ or 2 . They can be rewritten as 1 antisymmetric one, namely $(A_{12} - A_{21})/2$; and 3 symmetric ones, namely 1 trace $A_{11} + A_{22}$, 1 normal difference $A_{11} - A_{22}$, 1 off-diagonal terms $(A_{12} + A_{21})/2$. This means that an antisymmetric matrix has 1 independent component, a symmetric matrix has 3, a deviatoric one has 2, an isotropic one has 1.

The scalar product between matrices is $\bar{A}:\bar{B} = \sum_{i,j} A_{ij} B_{ij}$. The (“euclidian”) *norm* of \bar{A} is a strictly positive number

defined in any dimension D as:

$$\|\bar{A}\| = \sqrt{\bar{A}:\bar{A}} = \left[\sum_{i,j} (A_{ij}A_{ji}) \right]^{1/2}. \quad (46)$$

B.2 Diagonalisation

Any symmetric matrix \bar{S} can be diagonalised. That is, there exist three orthogonal axes, called \bar{S} 's *eigenvectors* (from the German word "eigen", meaning "own"), in which \bar{S} would be diagonal, see for instance eq. (4). That is, if we use these axes (instead of the original ones) to measure the matrix, it would have non-zero terms only along its diagonal:

$$\text{diag } \bar{S} = \begin{pmatrix} s_1 & 0 & 0 \\ 0 & s_2 & 0 \\ 0 & 0 & s_3 \end{pmatrix}. \quad (47)$$

The three numbers s_1, s_2, s_3 are called the matrix' *eigenvalues*.

They determine many properties of \bar{S} , including its trace and norm:

$$\begin{aligned} \text{Tr}(\bar{S}) &= s_1 + s_2 + s_3, \\ \|\bar{S}\| &= \sqrt{s_1^2 + s_2^2 + s_3^2}. \end{aligned} \quad (48)$$

If the s_i s are non zero, the inverse of \bar{S} exists, and it is diagonal in the same axes as \bar{S} :

$$\text{diag } \bar{S}^{-1} = \begin{pmatrix} \frac{1}{s_1} & 0 & 0 \\ 0 & \frac{1}{s_2} & 0 \\ 0 & 0 & \frac{1}{s_3} \end{pmatrix}. \quad (49)$$

If the s_i s are strictly positive, the *logarithm* of \bar{S} (see eq. 15) is defined by rotating to the eigenvectors, taking the logarithm of the eigenvalue, and rotate back to the original axes. By construction, $\log(\bar{S})$ is symmetric too (see eq. 16), and diagonal in the same axes as \bar{S} .

The literature of mechanics [23,33] sometimes uses a specific definition adapted for shear. A shear is characterised by a deviatoric matrix with two opposite eigenvalues ($s_1 = -s_2 = S$) and nothing in the third direction ($s_3 = 0$). Its *amplitude* S is defined as:

$$S = \left[\frac{1}{2} \sum_{i,j} S_{ij}^2 \right]^{1/2} = \frac{\|\bar{S}\|}{\sqrt{2}}. \quad (50)$$

B.3 Outer product

The *outer product* of two vectors \mathbf{a}, \mathbf{b} is the matrix of components $a_i b_j$:

$$\mathbf{a} \otimes \mathbf{b} = \begin{pmatrix} a_1 b_1 & a_1 b_2 & a_1 b_3 \\ a_2 b_1 & a_2 b_2 & a_2 b_3 \\ a_3 b_1 & a_3 b_2 & a_3 b_3 \end{pmatrix}. \quad (51)$$

Its trace is the scalar product $\mathbf{a} \cdot \mathbf{b} = a_1 b_1 + a_2 b_2 + a_3 b_3$.

In the text, the outer product appears for instance for the vector $\boldsymbol{\ell}$ (eq. 9). It is also used for the notation $\nabla = (\partial r_i) = (\partial/\partial x, \partial/\partial y, \partial/\partial z)$ (called gradient, or *nabla*) which symbolises the space derivatives:

$$\begin{aligned} \bar{\nabla} v &= \nabla \otimes \mathbf{v} = \frac{\partial v_j}{\partial r_i} \\ &= \begin{pmatrix} \frac{\partial v_1}{\partial x} & \frac{\partial v_2}{\partial x} & \frac{\partial v_3}{\partial x} \\ \frac{\partial v_1}{\partial y} & \frac{\partial v_2}{\partial y} & \frac{\partial v_3}{\partial y} \\ \frac{\partial v_1}{\partial z} & \frac{\partial v_2}{\partial z} & \frac{\partial v_3}{\partial z} \end{pmatrix} \end{aligned} \quad (52)$$

More precisely, eq. (24) uses its transposed:

$$\bar{\nabla} v = {}^t \frac{\partial v_i}{\partial r_j}. \quad (53)$$

Similarly, the rotational is the vector product $\nabla_i \times v_j$.

However, rheologists [23,33] often prefers the notation $\text{grad} v = \partial v_i / \partial r_j$. This creates an ambiguity with eqs. (52,53). In case of doubt, it is safe to come back to indices, which are unambiguous. For instance, the demonstration of eq. (29) writes as follows:

$$\frac{\partial \ell_i}{\partial t} = v_i(r_j + \ell_j) - v_i(r_j) = \sum_j \frac{\partial v_i}{\partial r_j} \ell_j. \quad (54)$$

For a rank three tensor, the notation $\bar{J} = \mathbf{v} \otimes \bar{M}$ means $J_{ijk} = v_i M_{jk}$, and the notation $\nabla \cdot \bar{J}$ is equivalent to $\sum_i \partial J_{ijk} / \partial r_i$.

B.4 Texture and stress

This appendix, inspired from ref. [9], aims at relating the texture with the stress; the matrices with their mathematical interpretation; and the discrete description with the continuous one.

Consider a pattern made of discrete objects. Now, draw a plane through the pattern, and note \mathbf{n} the vector normal to this plane. Some links $\boldsymbol{\ell}$ cut this plane, with a probability proportional to $\boldsymbol{\ell} \cdot \mathbf{n} = \ell_j n_j$ (where $\boldsymbol{\ell}$ is oriented by the direction of \mathbf{n} , so that this number is positive). It is higher for links which are long, and/or perpendicular to the plane. Thus the distribution of the $\boldsymbol{\ell}$ s which cut this plane is biased with respect to the distribution of $\boldsymbol{\ell}$ in the bulk.

More precisely, the average of the $\boldsymbol{\ell}$ s which cut this plane is $\langle \ell_i \ell_j n_j \rangle = M_{ij} n_j$, or equivalently $\bar{M} \cdot \mathbf{n}$. Thus \bar{M} can be interpreted as a tensor acting on the vector \mathbf{n} , to estimate the average of the $\boldsymbol{\ell}$ s crossing a plane normal to \mathbf{n} .

In that case, the outer product by $\boldsymbol{\ell}$ transforms the surface integral of a discrete individual vector, the link, into a bulk integral of a continuous average matrix, the texture. The discrete individual vector $\boldsymbol{\ell}$ encodes the information over the link and the corresponding continuous, statistical matrix is the average of $\boldsymbol{\ell} \otimes \boldsymbol{\ell}$. In this continuous

description, the orientation of ℓ does not play a role any longer, and the discrete pattern can be forgotten.

Eq. (9) is reminiscent of another application of the outer product, regarding stress [9,10,12]. Consider an assembly of particles which interact through a pairwise force \mathbf{F} , which we orient in the same direction as ℓ . The force through a plane of normal \mathbf{n} is proportional to:

$$\langle F_i \ell_j n_j \rangle = \langle \mathbf{F} \otimes \ell \rangle \cdot \mathbf{n}.$$

This means that the stress in this assembly is proportional (up to a prefactor, namely the density of links) to $\langle \mathbf{F} \otimes \ell \rangle$. As required, it is insensitive to the orientation of \mathbf{F} and ℓ . In that case, the outer product by ℓ transforms the surface integral of a discrete individual vector, the force, into a bulk integral of a continuous average matrix, the stress. The role that stress plays for force (continuous equivalent of a discrete description), \bar{M} plays it for the links themselves.

In the particular case of polymers or springs (with zero length at rest) where \mathbf{F} is proportional to ℓ , the stress is proportional to the texture. In foams, where forces are very different (and regard bubble walls rather than links between centers), there is no simple relation between them, as discussed in detail in ref. [12].

C Time evolution of the texture

C.1 Taking into account the finite number of links

This appendix can be useful for a user who wants to analyse a movie (and not only a static image). It helps to understand the definitions, units and measurements of \bar{C} and \bar{G} ; as well as the time evolution of \bar{M} (eq. 10).

We consider a movie, and more specifically two consecutive images at times t and $t + \Delta t$. If possible, Δt should be chosen small enough to enable a good sampling (as will become clear below); still, the average can be performed on a large time interval τ , that is, a large number $\tau/\Delta t$ of images. Measurements should not depend too much on the exact value of Δt . Thus most users can consider Δt as a prefactor, important only when comparing different experiments or simulations.

For a given quantity x which depends both on space and time, $\Delta x/\Delta t$ tends towards its partial time derivative $\partial x/\partial t$, since we perform all measurements in a fixed region of space (so-called ‘‘Eulerian’’ point of view, often useful in practice). In principle, if the measurement box moved with the links (so-called ‘‘Lagrangian’’ point of view, often useful in theory), $\Delta x/\Delta t$ would tend towards its usual time derivative dx/dt .

Eq. (38) can be rewritten as:

$$N_{tot} \bar{M} = \sum w \ell \otimes \ell. \quad (55)$$

Its variation between successive images, divided by Δt , involves the links ℓ_a (resp. ℓ_d) appeared (resp. disappeared)

during Δt :

$$\begin{aligned} \frac{\Delta(N_{tot} \bar{M})}{\Delta t} &= \sum \frac{\Delta w}{\Delta t} (\ell \otimes \ell) \\ &+ \sum w \left(\ell \otimes \frac{\Delta \ell}{\Delta t} + \frac{\Delta \ell}{\Delta t} \otimes \ell \right) \\ &+ \frac{1}{\Delta t} \left(\sum_a w_a \ell_a \otimes \ell_a - \sum_d w_d \ell_d \otimes \ell_d \right). \end{aligned} \quad (56)$$

Dividing both sides by N_{tot} yields:

$$\begin{aligned} \frac{\Delta \bar{M}}{\Delta t} + \bar{M} \frac{\Delta \log N_{tot}}{\Delta t} &= -\nabla \cdot \bar{J}_M \\ &+ \left(\bar{C} + \bar{C}^t \right) + \bar{T} \end{aligned} \quad (57)$$

The advection term $-\nabla \cdot \bar{J}_M$ is the term in $\Delta w/\Delta t$, in eq. (56). It is due to links entering or exiting the region where \bar{M} is measured. In a first approximation, $\bar{J}_M \simeq \mathbf{v} \otimes \bar{M}$: the demonstration is delicate and we do not develop it here (briefly: when the averaging procedure uses a coarse-graining function $w(\mathbf{r}(t))$, it is possible to transform a time derivative of w into a space derivative; this involves $d\mathbf{r}/dt$, that is, the local velocity [27,17]). We do not consider here in detail the influence of advection.

We also neglect here the influence of the variation of $\log N_{tot}$: if the movie has been correctly sampled, that is if Δt is small enough, the proportion of links created or destroyed during Δt remains small.

The geometrical variation term is:

$$\bar{C} = \frac{N_c}{N_{tot}} \left\langle \ell \otimes \frac{\Delta \ell}{\Delta t} \right\rangle. \quad (58)$$

Here N_c the number of links conserved between both images, that is, the number of terms involved in the average noted $\langle \cdot \rangle$ (hence the correction N_c/N_{tot}). If Δt is small enough, then $\Delta \ell/\Delta t$ tends towards $d\ell/dt$ and N_c/N_{tot} tends towards 1, so that we obtain eq. (12).

The topological term is between the last parentheses in eq. (56). Note that we can derive its exact prefactor (often unimportant in practice):

$$\bar{T} = \frac{1}{\Delta t} \frac{\Delta N_a}{N_{tot}} \langle \ell_a \otimes \ell_a \rangle - \frac{1}{\Delta t} \frac{\Delta N_d}{N_{tot}} \langle \ell_d \otimes \ell_d \rangle, \quad (59)$$

where ΔN_d is the number of disappeared links (that exist at t but no longer at $t + \Delta t$); and ΔN_a the number of appeared links (that exist at $t + \Delta t$ but not yet at t). In the limit of small Δt , eq. (59) tends towards eq. (13). In eq. (59), the number of terms involved in the average $\langle \ell_a \otimes \ell_a \rangle$ (resp. $\langle \ell_d \otimes \ell_d \rangle$) is ΔN_a (resp. ΔN_d), which is much smaller than N_{tot} : thus statistics on \bar{T} are always much noisier than that on \bar{M} or \bar{C} . It is thus advisable to integrate \bar{T} over a long time τ .

C.2 Objective derivatives

This technical section is rather aimed at specialists. It discusses the different objective derivatives which appear in the course of this paper, when estimating the time derivatives of $\bar{\bar{M}}$ or $\bar{\bar{U}}$.

C.2.1 Time evolution of $\bar{\bar{M}}$

In the affine assumption, the geometrical term $\bar{\bar{C}} + \bar{\bar{C}}^t$ of eq. (10) can be rewritten using eq. (19,31):

$$\begin{aligned} \bar{\bar{C}} + \bar{\bar{C}}^t &= \bar{\bar{M}} \cdot \bar{\bar{G}} + \bar{\bar{G}}^t \cdot \bar{\bar{M}} \\ &\stackrel{\text{affine}}{\simeq} \bar{\bar{M}} \cdot \bar{\nabla} v + \bar{\nabla} v^t \cdot \bar{\bar{M}}. \end{aligned} \quad (60)$$

Thus, the second term of the right hand side of eq. (10) can be grouped with its left hand side formally appearing as a Maxwell upper convective tensor derivative (see e.g [34]):

$$\bar{\nabla} \bar{\bar{M}} = \frac{\partial \bar{\bar{M}}}{\partial t} + v \cdot \nabla \bar{\bar{M}} - \bar{\nabla} v^t \cdot \bar{\bar{M}} - \bar{\bar{M}} \cdot \bar{\nabla} v. \quad (61)$$

Hence eq. (10) appears as a conservation equation for $\bar{\bar{M}}$:

$$\bar{\nabla} \bar{\bar{M}} \stackrel{\text{affine}}{\simeq} -\bar{\bar{T}}, \quad (62)$$

which source $\bar{\bar{T}}$ is due to topological changes. Note that the present approach has unambiguously selected the *upper* (rather than the lower, or any other) convective tensor derivative.

C.2.2 The small $\bar{\bar{U}}$ assumption

Consider now the case where the deformation $\bar{\bar{U}}$ is small everywhere. Inverting eq. (16), the texture develops as:

$$\begin{aligned} \bar{\bar{M}} &= \bar{\bar{M}}_0 \exp\left(2\bar{\bar{U}}\right) \\ &= \bar{\bar{M}}_0 \left(\bar{\bar{I}} + 2\bar{\bar{U}} + \mathcal{O}(\bar{\bar{U}}^2) \right) \\ &\stackrel{\text{small}}{\simeq} \bar{\bar{M}}_0 + 2\bar{\bar{M}}_0 \bar{\bar{U}}. \end{aligned}$$

This assumption is valid for foams, since the deformation of bubbles does not exceed the size of two bubbles before topological changes occurs, and thus $\|\bar{\bar{U}}\|$ is bounded. Let us also suppose that $\bar{\bar{M}}_0 = m_0 \bar{\bar{I}}$, *i.e.* that the reference configuration is isotropic. Then, eq. (62) becomes:

$$2m_0 \left(\bar{\nabla} \bar{\bar{U}} - \frac{\bar{\nabla} v + \bar{\nabla} v^t}{2} \right) \stackrel{\text{small}}{\simeq} -\bar{\bar{T}},$$

or equivalently:

$$\frac{\bar{\nabla} v + \bar{\nabla} v^t}{2} \stackrel{\text{small}}{\simeq} \bar{\nabla} \bar{\bar{U}} + \bar{\bar{P}}, \quad (63)$$

where $\bar{\bar{P}} = -\bar{\bar{T}}/(2m_0)$ denotes the rate of the plastic deformation. This linear assumption thus simplifies eqs. (66,23). Again, this selects an *upper* convective tensor derivative.

C.2.3 Kinematic equation of $\bar{\bar{U}}$

As in appendix C.2.2, we first invert the definition of $\bar{\bar{U}}$ (eq. 16):

$$\bar{\bar{M}} = \bar{\bar{M}}_0 \exp\left(2\bar{\bar{U}}\right). \quad (64)$$

We differentiate eq. (64), inject it in the time evolution of $\bar{\bar{M}}$ (eq. 10), then eliminate $\bar{\bar{M}}$ using eq. (16). We finally obtain the time evolution of $\bar{\bar{U}}$, *versus* $\bar{\bar{U}}$ instead of $\bar{\bar{M}}$. The complete calculation of this kinematical equation is heavy (in particular because it involves the rotation of the eigenvectors), and we do not develop it here. We only use its lowest order terms in $\bar{\bar{U}}$:

$$\begin{aligned} \frac{\partial \bar{\bar{U}}}{\partial t} &= -\bar{\nabla} \cdot \bar{\bar{J}}_U + \bar{\bar{V}} - \bar{\bar{\Omega}} \bar{\bar{U}} \\ &\quad - \bar{\bar{U}} \bar{\bar{\Omega}}^t + \mathcal{O}\left(\bar{\bar{U}}^2\right) - \bar{\bar{P}}. \end{aligned} \quad (65)$$

The term $-\bar{\bar{P}}$ appears on the r.h.s. thanks to the factor $-1/2$ in eq. (22). The $\mathcal{O}(\bar{\bar{U}}^2)$ term is often negligible in a plastic material such as considered here, where the elastic internal deformation is seldom much larger than unity.

On the other hand, the advection term $\bar{\bar{J}}_U$ and the rotation term $\bar{\bar{\Omega}} \bar{\bar{U}} + \bar{\bar{U}} \bar{\bar{\Omega}}^t$ have symmetries which are different from that of $\bar{\bar{V}}$ and $\bar{\bar{P}}$, and may not necessarily be negligible. They can be regrouped using the total *corotational* (“Jaumann” [35]) objective derivative:

$$\frac{\mathcal{D} \bar{\bar{U}}}{\mathcal{D} t} = \frac{\partial \bar{\bar{U}}}{\partial t} + \bar{\nabla} \cdot \bar{\bar{J}}_U + \bar{\bar{\Omega}} \bar{\bar{U}} - \bar{\bar{U}} \bar{\bar{\Omega}}^t, \quad (66)$$

where we recall that $\bar{\bar{\Omega}}^t = -\bar{\bar{\Omega}}$. We thus approximately obtain eq. (23).

References

1. C. Raufaste, unpublished (2007)
2. C. Quilliet, M. Idiart, B. Dollet, L. Berthier, A. Yekini, *Colloids and Surfaces A* **263**, 95 (2005)
3. G. Durand, F. Graner, J. Weiss, *Europhys. Lett.* **67**, 1038 (2004)
4. S. Courty, Y. Bellaïche, F. Graner, in preparation

5. M. Saint Jean, C. Guthmann, G. Couplier, *Eur. Phys. J. B* **39**, 61 (2004)
6. G. Couplier, M.S. Jean, C. Guthmann, *Phys. Rev. E* **73**(3), 031112 (2006)
7. A. Tanguy, F. Leonforte, J.L. Barrat, *Eur. Phys. J. E* **20**, 355 (2006)
8. K. Mecke, D. Stoyan, eds., *Morphology of Condensed Matter - Physics and Geometry of Spatially Complex Systems*, Lecture Notes in Physics 600 (Springer, Heidelberg, 2002)
9. M. Aubouy, Y. Jiang, J.A. Glazier, F. Graner, *Granular Matt.* **5**, 67 (2003)
10. M. Asipauskas, M. Aubouy, J.A. Glazier, F. Graner, Y. Jiang, *Granular Matt.* **5**, 71 (2003)
11. S. Courty, B. Dollet, F. Elias, P. Heinig, F. Graner, *Europhys. Lett.* **64**, 709 (2003)
12. E. Janiaud, F. Graner, *J. Fluid Mech.* **532**, 243 (2005)
13. B. Dollet, M. Aubouy, F. Graner, *Phys. Rev. Lett.* **95**, 168303 (2005)
14. B. Dollet, F. Graner, *J. Fluid Mech.* **585**, 181 (2007)
15. P. Marmottant, C. Raufaste, F. Graner, preprint
16. D. Weaire, S. Hutzler, *The physics of foams* (Oxford University Press, Oxford, 1999)
17. B. Dollet, Ph.D. thesis, Université Grenoble I (2005)
18. D. Weaire, N. Rivier, *Contemp. Phys.* **25**, 59 (1984)
19. H. Ohlenbusch, T. Aste, B. Dubertret, N. Rivier, *Eur. Phys. J B* p. 211 (1998)
20. B. Dubertret, T. Aste, H. Ohlenbusch, N. Rivier, *Phys. Rev. E* **58**, 6368 (1998)
21. G.K. Batchelor, *An introduction to fluid dynamics* (Cambridge University Press, Cambridge, 2000)
22. L.D. Landau, E.M. Lifchitz, *Theory of elasticity* (Reed, 1986)
23. J. Chakrabarty, *Theory of plasticity* (McGraw-Hill Book Company, New York, 1978)
24. R. Tanner, E. Tanner, *Rheologica Acta* **42**(1 - 2), 93 (2003)
25. A. Hoger, *International Journal of Solids and Structures* **23**(12), 1645 (1987)
26. N. Kruyt, *Int. J. Solids Struct.* **40**, 511 (2003)
27. I. Goldhirsch, C. Goldenberg, *Eur. Phys. J. E* **9**(3), 245 (2002)
28. A.N. Beris, J.A. Tsamopoulos, R.C. Armstrong, R.A. Brown, *J. Fluid Mech.* **158**, 219 (1985)
29. J. Blackery, E. Mitsoulis, *J. Non-Newt. Fluid Mech.* **70**(1-2), 59 (1997)
30. P. Marmottant, F. Graner, accepted for *Eur. Phys. J. E* (2007)
31. Extract from the anonymous referee report to [9]
32. A.F.M. Marée, V.A. Grieneisen, P. Hogeweg, in *Single Cell Based Models in Biology and Medicine*, edited by A.R.A. Anderson, M.A.J. Chaplain, K.A. Rejniak (Birkhäuser-Verlag, Basel, 2007), pp. 107–136
33. D. François, A. Pineau, A. Zaoui, *Comportement mécanique des matériaux : élasticité et plasticité* (Hermès, 1995)
34. C.W. Macosko, *Rheology : principles, measurements and applications* (Wiley-VCH, 1994)
35. H. Pleiner, M. Liu, H. Brand, *Rheologica Acta* **43**, 502 (2004)